

Towards an enhanced metric for detecting vertical flow decoupling in eddy covariance flux observations

Olli Peltola ^{a,b,*}, Toprak Aslan ^b, Mika Aurela ^b, Annalea Lohila ^{b,c}, Ivan Mammarella ^c, Dario Papale ^{d,e}, Christoph K. Thomas ^{f,g}, Timo Vesala ^{c,h}, Tuomas Laurila ^b

^a Natural Resources Institute Finland (Luke), Latokartanonkaari 9, Helsinki, 00790, Finland

^b Climate Research Programme, Finnish Meteorological Institute, P.O. Box 503, 00101, Helsinki, Finland

^c Institute for Atmospheric and Earth System Research/Physics, Faculty of Science, University of Helsinki, P.O. Box 68, 00014, Helsinki, Finland

^d Institute of Research on Terrestrial Ecosystems (IRET) National Research Council (CNR), 00015, Monterotondo (Roma), Italy

^e IAFES, euroMediterranean Center on Climate Change (CMCC), 01100, Viterbo, Italy

^f Micrometeorology Group, University of Bayreuth, Bayreuth, Germany

^g Bayreuth Center for Ecology and Environmental Research, BayCEER, University of Bayreuth, Bayreuth, Germany

^h Institute for Atmospheric and Earth System Research/Forest Sciences, Faculty of Agriculture and Forestry, University of Helsinki, P.O. Box 27, 00014, Helsinki, Finland

ARTICLE INFO

Dataset link: <https://doi.org/10.5281/zenodo.14259134>, https://github.com/OPeltola/EC_Omega_filtering

Keywords:
 Decoupling
 Gas flux
 Eddy covariance
 Vertical mixing
 Canopy drag
 Stable stratification

ABSTRACT

The eddy covariance (EC) technique has emerged as the method of choice for observing ecosystem–atmosphere interactions across biomes and climate zones. However, EC measurements are biased when the turbulent flow is decoupled from the underlying surface, severely limiting the applicability of the technique in observing surface–atmosphere fluxes. Friction velocity (u_*) is typically used to detect and filter these periods from EC flux time series. The processes that control decoupling are understood qualitatively, including the strength of vertical turbulent mixing, stable stratification and canopy drag. However, the standard practice utilising u_* misses most of these processes, resulting in a significant uncertainty in detecting decoupling. Consequently, a quantitative metric, Ω , which encapsulates all these processes in a unified framework, was recently proposed. However, it has not yet been systematically tested over a range of ecosystems and site characteristics. The objectives of this study were therefore to test the efficacy of Ω at a diverse range of EC sites, to quantify the processes controlling decoupling across sites, and to compare Ω against other decoupling metrics, such as u_* . A similar Ω threshold value for coupling was observed at all the 45 tested EC sites, with a value of 0.66 ± 0.06 (mean \pm standard deviation). This indicates that the Ω metric captured the essential features of decoupling across sites, thereby enabling deeper analyzes of the causes of decoupling. For example, Ω indicates that (1) flows above dense forest canopies can be decoupled from the forest floor also during the daytime due to canopy drag and that (2) during stable stratification decoupling is more likely with tall towers. These findings significantly enhance our scientific understanding of the underlying causes of decoupling, will inform improved analyzes of EC data and support near-surface turbulence transport analyzes in open and forested landscapes.

1. Introduction

Human activities and the rapidly changing climate are causing unprecedented changes to global biomes and knowledge of these changes is insufficient, primarily due to uncertainty of processes involved and lack of suitable measurements to constrain process models (e.g. [Arneth et al., 2017](#); [Huntzinger et al., 2017](#)). During the recent decades the eddy covariance (EC) technique has emerged as the method of choice for observing the exchange of gases, heat and momentum between ecosystems and the atmosphere ([Baldocchi, 2020](#)) at the ecosystem

scale across biomes and climate zones. Consequently, the global flux measurement network (FLUXNET) has a key role in improving our understanding on ecosystem–atmosphere interactions and changes in these interactions in a changing climate. Furthermore, EC observations form the backbone of several long-term research infrastructures such as Integrated Carbon Observation System (ICOS; [Franz et al. \(2018\)](#), [Heiskanen et al. \(2022\)](#)) and National Ecological Observatory Network (NEON; [Metzger et al. \(2019\)](#)) to name a few.

Despite its pivotal role in monitoring ecosystem–atmosphere interactions, the fluxes measured with the EC technique do not always relate

* Corresponding author at: Natural Resources Institute Finland (Luke), Latokartanonkaari 9, Helsinki, 00790, Finland.
 E-mail address: olli.peltola@luke.fi (O. Peltola).

to ecosystem–atmosphere exchange, especially during low turbulent mixing periods taking place primarily at night (e.g. Aubinet et al., 2012). EC relies on the observation of vertical turbulent flux of a constituent c (e.g. carbon dioxide, CO₂). Mass balance of a control volume on top of a target ecosystem reads

$$NEE = F_c + S_c + F_{htfd} + F_{hadv} + F_{vadv} = F_c + S_c + F_{res}, \quad (1)$$

where NEE is the net ecosystem exchange of c , F_c is the vertical turbulent flux, S_c is the change in storage term and F_{res} is the sum of horizontal turbulent flux divergence (F_{htfd}) and horizontal (F_{hadv}) and vertical (F_{vadv}) advection (e.g. Finnigan et al., 2003; Foken et al., 2012). At many EC sites S_c is measured along with F_c , however the terms lumped in F_{res} are unmeasurable with current techniques (e.g. Leuning et al., 2008; Aubinet et al., 2010). During rigorous turbulent mixing, the approximation $NEE \approx F_c$ (or $NEE \approx F_c + S_c$) holds and EC measurements can be used to monitor NEE (but see Katul et al. (2006), Poggi and Katul (2007), Ross (2011), Ross and Harman (2015), Kanani-Sühring and Raasch (2015, 2017), Chen et al. (2019), Ma et al. (2020)). However, during low mixing the turbulent flow decouples from the surface since vertical mixing is resisted by strong vertical movement opposing forces such as buoyancy and canopy drag (Peltola et al., 2021b), F_{res} becomes important and hence EC observations depart from the ecosystem–atmosphere exchange (i.e. NEE) (e.g. Aubinet, 2008; Feigenwinter et al., 2008; Leuning et al., 2008; Aubinet et al., 2010; Feigenwinter et al., 2010). As a result, EC observations can be severely biased if not handled correctly and this can result e.g. in biased ecosystem carbon balance estimates due to underestimated nocturnal ecosystem respiration (e.g. Platter et al., 2024). This issue is still largely debated despite decades of studies on the subject (Aubinet et al., 2003; Feigenwinter et al., 2004; Aubinet et al., 2005; Marcolla et al., 2005; Staebler and Fitzjarrald, 2004; Mammarella et al., 2007; Aubinet, 2008; Feigenwinter et al., 2008; Kutsch et al., 2008; Leuning et al., 2008; Aubinet et al., 2010; Feigenwinter et al., 2010; Thomas, 2011; Siebicke et al., 2012; Vickers et al., 2012; Galvagno et al., 2017; Rannik et al., 2020) and it arguably forms one of the main hindrances for the accuracy of EC observations.

A pragmatic approach to overcome this problem has been to filter out the low turbulence periods from EC time series. These periods are typically identified using friction velocity (u_*) (Goulden et al., 1996; Gu et al., 2005; Reichstein et al., 2005; Papale et al., 2006; Aubinet et al., 2012; Barr et al., 2013; Wutzler et al., 2018; Pastorello et al., 2020) which assumes that the density normalised shear induced momentum flux is a good indicator for the resulting effective mixing strength for the entire air column below the EC setup. Another assumption at the basis of u_* filtering is that nighttime NEE , representing only respiration, is independent respect to the turbulence intensity (u_*) when the biological drivers are similar (e.g. temperature, water availability, substrate). Under low turbulence conditions this independence is not any more present and this is used to estimate a minimum level of turbulence (u_* threshold, u_{*th}) needed to consider the EC observations representative of ecosystem–atmosphere interactions. All the measurements collected at u_* values below the threshold are removed because they are considered to be affected by potential advection. This approach views the problem from a biological standpoint and evaluates the best available estimate for nocturnal NEE (typically $F_c + S_c$) against turbulence metrics such as u_* . Determination of the site-specific u_{*th} is uncertain and this uncertainty dominates the overall uncertainty of EC observations (Papale et al., 2006; Wutzler et al., 2018; Pastorello et al., 2020).

However, the use of u_* , square root of momentum flux, as a filtering metric can be challenged from a fluid dynamics standpoint. For instance, in forested landscapes majority of momentum flux between the atmosphere and the underlying ecosystem is related to the upper parts of the forest canopy represented e.g. by the roughness of the canopy crowns, their spacing, their differences in height etc. (e.g. Finnigan, 2000; Yi, 2008; Brunet, 2020) and hence u_* does not relate

to the fact that whether the above-canopy turbulent flow is in direct interaction with the forest floor or not (see also van Gorsel et al., 2011; Thomas et al., 2013). Furthermore, its values can be contaminated by non-turbulent large scale motions not directly related to local conditions (Acevedo et al., 2009). The selection of u_* as a low turbulence metric can be considered merely as a practical choice, since u_* observations are available at all EC sites, lacking a strong physical justification (Vickers et al., 2012). Hence alternative approaches including comparison of flow statistics across multiple levels of flux measurements have been proposed as well (Van Gorsel et al., 2007; Mammarella et al., 2007; Acevedo et al., 2009; van Gorsel et al., 2009; Vickers et al., 2012; Alekseychik et al., 2013; Thomas et al., 2013; Jocher et al., 2017; Freundorfer et al., 2019; Jocher et al., 2020; Schilperoort et al., 2020; Stiegler et al., 2023). However, these approaches also rely on site-specific threshold values and similarly to u_* typically lack a direct connection to forces hindering the vertical coupling with the exception of the multi-layer EC measurement studies (Freundorfer et al., 2019; Thomas et al., 2013). However, even the latter make use of evaluating the flow statistics at distinct heights where observations are available and not continuously throughout the canopy profile and rely only on vertical turbulent kinetic energy (TKE) observations. Some of the above-mentioned studies used standard deviation of vertical wind speed component (σ_w , square root of vertical TKE) as a filtering metric instead of u_* and estimated the σ_w threshold from comparison between subsequent above- and below-canopy turbulence measurements. However, difference between this approach and the approach based on u_* is likely marginal as u_* and σ_w are tightly correlated and follow linear dependence ($\sigma_w \approx 1.25u_*$) over a wide range of atmospheric stability conditions and ecosystem types (Kaimal and Finnigan, 1994).

These deficiencies of commonly used approaches motivated Peltola et al. (2021b) to develop a physics-based alternative for the u_* filtering. Their decoupling metric Ω incorporates the vertical turbulent kinetic energy and the forces hindering vertical movement, i.e. buoyancy and canopy drag, hence providing possibly more rigorous scientific basis for identifying periods when the turbulent flow is not coupled with the surface and hence EC measurements do not represent NEE . Peltola et al. (2022) were able to track the growth of large canopy eddies as Ω increased and they observed attachment of these eddies to forest floor at specific Ω values partially validating the physical basis of the decoupling metric. However, their analyzes focused only on two sites and hence the main aim of this study is to evaluate the applicability of Ω in detecting flow decoupling above wide range of ecosystems and evaluate processes controlling decoupling. Furthermore, we evaluate whether Ω is suitable for delineating decoupling without site-specific thresholds and derive commonly applicable Ω threshold and its uncertainty. We leverage data from 45 flux sites spanning from deserts to agricultural grasslands and dense evergreen forests and compare Ω based filtering with the traditional approach using u_* and σ_w .

2. Materials and methods

2.1. Identifying flow decoupling with the metric Ω

For a thorough description of the decoupling metric Ω , see Peltola et al. (2021b), here only the main details are reiterated. The approach relies on the concept of downward moving air parcels and forces hindering their movement and is akin to the approach of Bougeault and Lacarrere (1989) for estimating turbulent mixing lengths implemented in some numerical weather prediction models (Lac et al., 2018; Maroneze et al., 2020). The movement of a downward moving air parcel at the canopy height (h) is hindered by canopy drag and buoyancy force. The work performed against these forces during the descent can be calculated as a line integral over the vertical trajectory assumed to be from $z = h$ to $z = 0$ m. The air parcel reaches the ground, e.g. forest floor, if its kinetic energy matches or exceeds this work. From

this, a minimum vertical speed ($w_{e,crit}$) required for the air parcel to reach the ground can be derived (see Peltola et al., 2021b):

$$w_{e,crit} = -\gamma \hat{c}_d PAIU_h - \sqrt{\left(\gamma \hat{c}_d PAIU_h\right)^2 + 2gh \frac{\theta_e - \hat{\theta}}{\hat{\theta}}}, \quad (2)$$

where $\gamma = 0.277$, c_d is drag coefficient (=0.2 throughout the study), PAI is one-sided plant area index ($m^2 m^{-2}$) describing the density of the forest canopy, U_h is mean wind speed at the canopy height ($m s^{-1}$), g is acceleration due to gravity ($m s^{-2}$), θ is potential temperature (K) and θ_e potential temperature of the air parcel which is assumed to be the same as the mean θ at its point of origin, i.e. canopy height. Hat ($\hat{\cdot}$) denotes average below h . When deriving Eq. (2), it was assumed that (1) humidity gradients are small meaning that buoyancy force can be calculated using θ , (2) canopy density and c_d are constant with height and that (3) mean horizontal wind speed and air parcel downward speed below canopy decay exponentially with height (e.g. Inoue, 1963; Cionco, 1965; Amiro, 1990; Poggi et al., 2004) and the coefficients controlling the decay are lumped in γ (Peltola et al., 2021b). γ was assumed constant for simplicity, however, the accuracy of this assumption can be questioned (see Brunet (2020) and references therein). Furthermore, $w_{e,crit}$ does not consider horizontal heterogeneity in canopy characteristics such as variability of PAI in different wind directions. Also, horizontal variability in temperature profiles is not accounted for and single temperature profile is assumed to sufficiently describe the study domain at each time step. Such temperature horizontal heterogeneity might prevail in heterogeneous forested ecosystems (Thomas, 2011) or other complex measurement locations such as lake shores (e.g. Jammet et al., 2017). In essence, Eq. (2) neglects any horizontal variability in PAI or temperature profiles and Ω is a metric for vertical decoupling only. Note that most of the assumptions made above are related to canopy drag and similar assumptions are often made when deriving simple models describing canopy flows (see e.g. Kunadi et al. (2024) and references therein). The assumptions were made in order to facilitate the calculation of Ω from a minimal set of micrometeorological measurements, i.e. turbulence at EC height and temperature profile below it. Despite these simplifications, we argue that Eq. (2) captures the essential features hindering vertical mixing. When $w_{e,crit}$ is imaginary, e.g. during unstable stratification, its value is set to zero.

By using Eq. (2) and standard deviation of vertical wind speed (σ_w), the decoupling metric Ω was defined as

$$\Omega = \frac{\sigma_w}{|w_{e,crit}|}. \quad (3)$$

Ω approaches infinity when the hindrances for the coupling are negligible, i.e. $|w_{e,crit}|$ approaches zero, and all the descending air parcels reach the ground. During weak turbulence σ_w is small when compared to $|w_{e,crit}|$ and hence Ω approaches zero and none of the air parcels reach the ground. A threshold for flow coupling can be determined somewhere between these two extremes. Peltola et al. (2021b) used $\Omega_{th} = 0.61$, but this threshold value will be re-evaluated in this study. If we assume Gaussian distribution for w fluctuations, then $\Omega_{th} = 0.61$ suggests that coupling takes place when over 5% of w fluctuations are below (i.e. stronger) the threshold $w_{e,crit}$ and hence reach and couple with the ground. Widely applicable universal Ω threshold for coupling might apply since Ω combines the main processes controlling vertical mixing in a single dimensionless metric and hence all EC measurement locations can be analyzed similarly. For a schematic description of Ω and processes controlling decoupling, see Fig. 1. Based on Ω , the flow can decouple from the ground if turbulent mixing (σ_w) decreases or hindrances for the vertical mixing ($|w_{e,crit}|$) increase. This latter part is missing from the more traditional low turbulence filtering metrics, i.e. u_* and σ_w . In practice, EC measurements are done at some distance above the canopy, see Peltola et al. (2021b) how this is taken into account in the calculation of Ω . In this study, canopy drag was approximated to have negligible contribution to $w_{e,crit}$ at low vegetation sites ($h < 1$ m) and was neglected when calculating $w_{e,crit}$ and Ω . Appendix B

shows how Ω is linked to different length scales used in prior studies to describe turbulent flows.

Various measurements are needed for calculating the decoupling metric Ω and these measurements can contain uncertainties which result in potentially erroneous values for Ω . Hence sensitivity of Ω to the accuracy of different input variables is evaluated in Appendix C. Also, a thumb rule describing the amount of temperature measurement levels needed for Ω calculation is derived.

2.2. Data sources and processing

In this study we leverage readily available data from EC measurement networks where all the needed variables are collected and shared, namely ICOS (Franz et al., 2018; Heiskanen et al., 2022) and NEON (Metzger et al., 2019) in addition to a few other sites. F_c and S_c were observed using standardised EC equipment and concentration profile measurements in each network. In total 45 sites were included. Site listing and characteristics are given in Table 1. In summary the sites range from short towers (3 to 8 m) above low vegetation to medium-height (20 to 30 m) and tall towers (30 to 60 m) above forests with various canopy densities (PAI between 0.5 and 9.4 $m^2 m^{-2}$). The ecosystem types range from deserts and grasslands to dense and tall forests and hence the sites cover the variability across typical EC towers. NEON EC and profile data (Metzger et al., 2017, 2019) were acquired from NEON data portal (National Ecological Observatory Network (NEON), 2023). One-sided PAI values calculated with HemiPy (Brown et al., 2023) from the NEON fisheye images (National Ecological Observatory Network (NEON), 2022) were retrieved from the Ground Based Observation for Validation service (Brown et al., 2020). Processed data (EC, profiles and PAI) (Sabbatini et al., 2018; Gielen et al., 2018) from the ICOS sites were retrieved from the ICOS carbon portal (see data citations in Table 1). Discontinuous PAI observations were linearly interpolated to match each EC data time step for sites with over five PAI observations, whereas at sites with less observations constant value was used. Long gaps (longer than three months) in PAI time series were filled with mean annual pattern. Handful of other sites were also included and data were processed by the site PIs.

Atmospheric stability was evaluated based on Monin–Obukhov stability parameter $\zeta = \frac{z_{EC}-d}{L}$ (Monin and Obukhov, 1954), where d and L are the displacement height and Obukhov length, respectively. d was approximated as $\frac{2}{3}h$ for sites for which it was not provided with the data. U_h was approximated from wind speed at the EC height (U) using Monin–Obukhov similarity scaling (Dyer, 1974):

$$U_h \approx U - \frac{u_* \phi_m}{k(z_{EC} - d)}(z_{EC} - h), \quad (4)$$

where k is von Kármán constant (=0.4) and ϕ_m is stability scaling function (Kaimal and Finnigan, 1994) estimated as $\phi_m = 1 + 5\zeta$ for stable conditions and for simplicity as $\phi_m = 1$ for unstable conditions.

Initial analyzes revealed systematic biases in the temperature profiles at some sites such as clearly different temperature values at certain height when compared to adjacent measurement heights. In order to minimise their effect on the calculation of Ω , they were rectified by assuming that in near-neutral situations θ does not strongly vary between adjacent measurement heights and then by cross-calibrating the measurement levels against each other using linear interpolation. Here near-neutral periods were defined as periods when the absolute value of above-canopy sensible heat flux was below 5 $W m^{-2}$ and friction velocity was above 0.5 $m s^{-1}$. If there were less than 100 data points that met these criteria, then the limits were loosened to 10 $W m^{-2}$ and 0.3 $m s^{-1}$, respectively. Data processing and analysis was done with Python (3.11.6) and scientific color maps were used in visualisations (Crameri et al., 2020).

Data quality filtering was done by site PIs or by centralised processing (ICOS/NEON). In addition, also the following periods were removed prior to analysis: $\sigma_w/u_* > 3$ or $\sigma_w/u_* < 0.5$ or $u_* > 2 m s^{-1}$ or $U >$

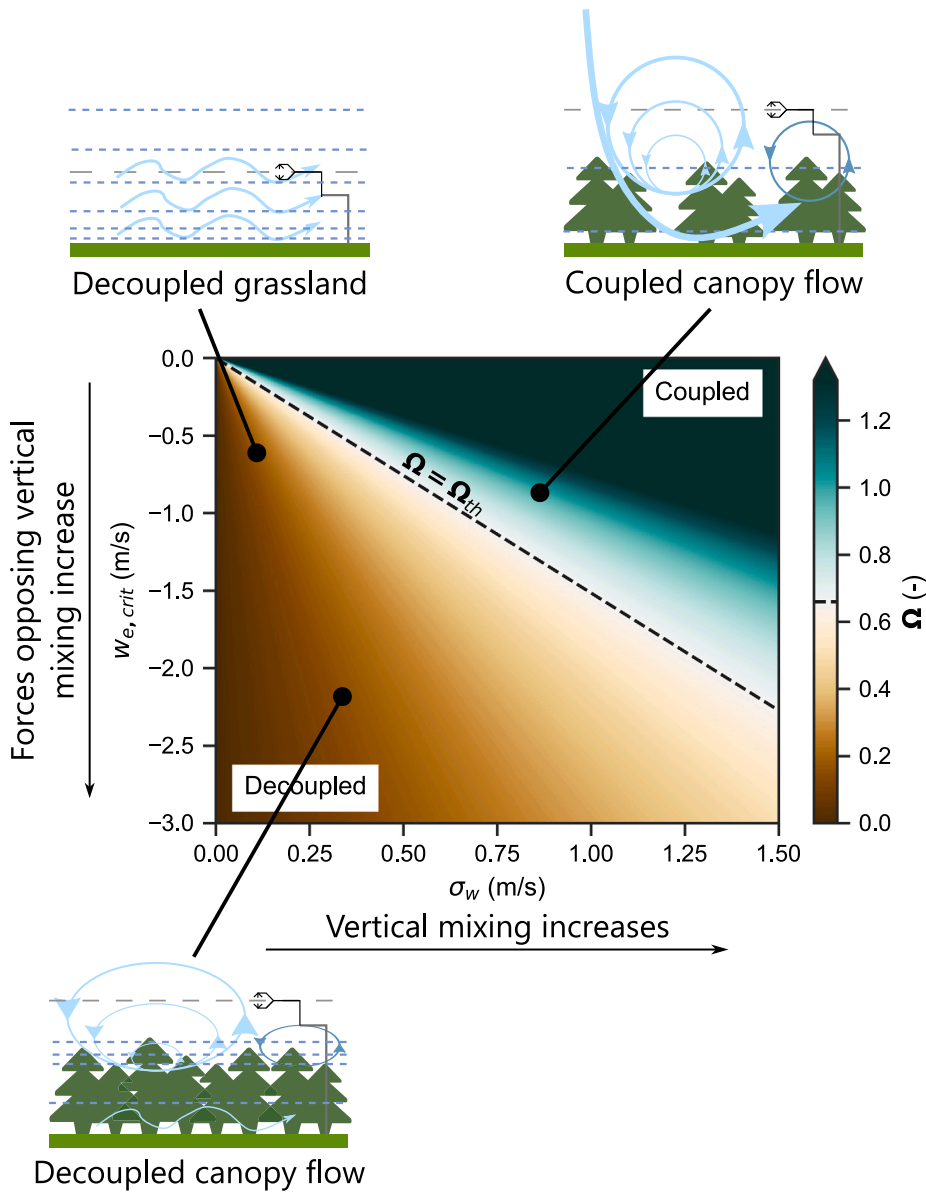


Fig. 1. Middle: Description on how Ω ($\Omega = \frac{\sigma_w}{|w_{e,crit}|}$) incorporates strength of vertical mixing and forces opposing vertical mixing in a single decoupling metric and how different coupling regimes (decoupled regime: $\Omega \in [0, \Omega_{th}]$; coupled regime: $\Omega \in (\Omega_{th}, \infty)$) depend on these two aspects. When $\Omega > \Omega_{th}$, then vertical mixing is strong enough for overcoming the hindrances for the coupling and the flow couples with the ground. Note that the traditional metrics for coupling (e.g. u_* or σ_w) vary only along the x-axis of this diagram and neglect any variability along the y-axis. Top and bottom: Three schematic illustrations on the flow in decoupled and coupled regimes.

20 m s⁻¹ or $F_c > 20 \mu\text{mol m}^{-2}\text{s}^{-1}$ or $F_c < -40 \mu\text{mol m}^{-2}\text{s}^{-1}$ or during night time $F_c < -10 \mu\text{mol m}^{-2}\text{s}^{-1}$. While F_c values below $-40 \mu\text{mol m}^{-2}\text{s}^{-1}$ are plausible, we observed only spurious outliers beyond these F_c limits and hence opted to remove them. After this filtering, the residual spikes in the 30-min flux time series were filtered using the algorithm proposed by Papale et al. (2006). Throughout the study, night time was defined as periods when global radiation was below 10 W m⁻².

In order to collapse nocturnal CO₂ fluxes across seasons and sites when plotting against decoupling metrics, we normalised fluxes with reference fluxes (F_{ref}) estimated by calculating 10-day running median of night time F_c data that were measured when u_* was above 75th percentile of night time u_* observed at each site. This approach assumes that (1) ecosystem respiration does not noticeably change with time scales shorter than 10 days and (2) the 75th percentile limit for u_* allows sufficiently accurate estimation of night time respiration. Due to these assumptions this gives only a rough estimate for the unbiased night time fluxes but most importantly the normalisation is independent of Ω . S_c was not included in the normalisation. Note

that the normalised fluxes were used only for illustration purposes in Section 3.1 and normalisation does not have an impact on the relative change in normalised flux against the decoupling metric, but only on the magnitude of F_c/F_{ref} and $(F_c + F_s)/F_{ref}$.

Friction velocity thresholds (u_{*th}) related to insufficient vertical mixing were derived for each site using the tool implemented in the ONEflux code package (Pastorello et al., 2020), specifically with the moving-point-transition approach. Shortly, the approach consists of two main steps: (1) the data are divided into categories based on season and air temperature. Within each season/temperature group the data are then divided into 20 u_* classes and bin-averages of fluxes in these u_* classes are calculated. (2) for each season/temperature group u_{*th} is selected from the u_* class in which the average flux reaches more than 99% of the average flux at the higher u_* classes and if this is valid also for the following u^* class in order to reduce noise effect. Then the median of the u_{*th} estimated for the same season at different temperature classes is calculated and the maximum threshold among the 4 seasons selected as final overall threshold value for that particular

Table 1

Eddy covariance measurement sites included in this study. For canopies with height below 1 m PAI are not reported as canopy drag is approximated to have insignificant influence on Ω at these locations. IGBP = vegetation IGBP classification. z_{EC} = EC measurement height above ground, h = canopy height and N = amount of half-hourly data points available. NEON = National Ecological Observatory Network (NEON) (2023). Significant slope = slope angle between 5% and 10%. Medium slope = slope angle between 2% and 5%.

ID	Reference	Latitude (°N)	Longitude (°E)	IGBP	z_{EC} (m)	h (m)	PAI($m^2 m^{-2}$)	Topography	Years	N (#)
CH-Dav	Gharun et al. (2020)	46.81533	9.85591	ENF	35	27	3.9	significant slope	2019...2020	9984
DE-Hai	Knöhl et al. (2021)	51.079407	10.452089	DBF	44	35	1.9...5.8	significant slope	2019...2020	26 155
DE-HoH	Rebmann et al. (2020)	52.085306	11.219222	DBF	45	33	1.2...5.1	significant slope	2019...2020	23 654
FI-Hyy	Mammarella et al. (2021)	61.84741	24.29477	ENF	27	21	2.1...3.6	hilly terrain	2018...2020	24 837
FI-Jok	Lohila et al. (2004)	60.8986	23.5134	GRA	3	<1	—	flat terrain	2002	10 359
FI-Ken	Aurela et al. (2015)	67.98728	24.28105	ENF	23	14.5	1.9	hilly terrain	2018...2021	28 255
FI-Sod	Thum et al. (2007)	67.3624	26.6386	ENF	24.5	12	1.2	flat terrain	2006...2008	30 045
FR-Aur	Tallec et al. (2021)	43.54965	1.106103	CRO	3	<1	—	medium slope	2019...2020	10 804
FR-Bil	Loustau et al. (2020)	44.493652	-0.956092	ENF	15.6	9.4	1.4	flat terrain	2019...2020	12 536
FR-Fon	Dufréne et al. (2020)	48.476357	2.780096	DBF	37	25	1.7...6.2	medium slope	2019...2020	15 070
IT-SR2	Arriga et al. (2020)	43.73202	10.29091	ENF	24.3	18	2.5	flat terrain	2019...2020	7514
PR-xGU	NEON	17.96955	-66.8687	EBF	20.1	6	1.4...4.2	hilly terrain	2019...2021	11 368
PR-xLA	NEON	18.021261	-67.076889	GRA	7.9	<1	—	flat terrain	2019...2021	9727
SE-Deg	Nilsson et al. (2020)	64.18203	19.55654	WET	3	<1	—	flat terrain	2019...2020	14 744
SE-Htm	Heliasz et al. (2020)	56.09763	13.41897	ENF	27	18	3.9...4.7	medium slope	2018...2020	38 886
SE-Nor	Mölder et al. (2020)	60.0865	17.479504	ENF	36	28	2.8	flat terrain	2018...2020	29 957
SE-Svb	Peichl et al. (2020)	64.25611	19.7745	ENF	34.5	20	3.4	sloped terrain	2019...2020	7161
US-MRF	Thomas et al. (2013)	44.646	-123.551	ENF	38	28	9.4	complex terrain	2006...2007	11 444
US-xAE	NEON	35.410599	-99.058779	GRA	7.9	<1	—	flat terrain	2019...2021	27 721
US-xBA	NEON	71.28241	-156.61936	WET	7.9	<1	—	flat terrain	2019...2021	8273
US-xBR	NEON	44.063889	-71.287375	DBF	35.4	20	1.0...6.2	hilly terrain	2019...2021	30 332
US-xCP	NEON	40.815536	-104.74559	GRA	7.9	<1	—	flat terrain	2019...2021	23 628
US-xDC	NEON	47.16165	-99.10656	GRA	7.9	<1	—	hilly terrain	2019...2021	35 243
US-xDL	NEON	32.541727	-87.803877	MF	42.1	30	0.7...5.3	flat terrain	2019...2021	14 574
US-xDS	NEON	28.12505	-81.43619	CVM	7.9	2	1.0...1.7	flat terrain	2019...2021	20 469
US-xHA	NEON	42.53691	-72.17265	DBF	38.7	23	2.3...4.9	hilly terrain	2019...2021	27 222
US-xHE	NEON	63.875798	-149.21335	OSH	7.9	<1	—	hilly terrain	2019...2021	20 587
US-xJE	NEON	31.194839	-84.468623	ENF	42.1	22	0.7...4.7	flat terrain	2019...2021	25 983
US-xJR	NEON	32.590694	-106.84254	OSH	7.9	<1	—	flat terrain	2019...2021	23 855
US-xKA	NEON	39.110446	-96.612935	GRA	7.9	<1	—	flat terrain	2019...2021	26 024
US-xKZ	NEON	39.100774	-96.563075	GRA	7.9	<1	—	hilly terrain	2019...2021	30 323
US-xMB	NEON	38.248283	-109.38827	OSH	7.9	<1	—	hilly terrain	2019...2021	22 391
US-xNG	NEON	46.76972	-100.91535	GRA	8	<1	—	flat terrain	2019...2021	26 804
US-xNQ	NEON	40.177599	-112.45245	OSH	7.9	<1	—	flat terrain	2019...2021	26 305
US-xNW	NEON	40.05425	-105.58237	ENF	8	<1	—	hilly terrain	2019...2021	16 441
US-xRN	NEON	35.964128	-84.282588	DBF	38.7	28	0.8...5.4	hilly terrain	2019...2021	24 238
US-xSB	NEON	29.689282	-81.993431	ENF	35.4	20	0.5...4.7	flat terrain	2019...2021	25 889
US-xSC	NEON	38.892925	-78.139494	DBF	52.1	30	0.5...6.6	hilly terrain	2019...2021	13 017
US-xSE	NEON	38.890131	-76.560014	DBF	62.2	37.2	0.6...5.6	flat terrain	2019...2021	28 121
US-xSL	NEON	40.461894	-103.02929	CRO	7.9	3	1.6	flat terrain	2019...2021	20 226
US-xSR	NEON	31.9107	-110.8355	OSH	7.9	<2	—	flat terrain	2019...2021	27 285
US-xST	NEON	45.50894	-89.58637	DBF	21.3	9.5	0.8...4.6	flat terrain	2019...2021	42 315
US-xTL	NEON	68.66109	-149.37047	WET	7.9	<1	—	hilly terrain	2019...2021	17 547
US-xUN	NEON	46.23391	-89.537254	MF	36.9	23	0.9...4.8	flat terrain	2019...2021	36 502
US-xWD	NEON	47.1282	-99.241334	GRA	7.9	<1	—	flat terrain	2019...2021	26 307

year (see Pastorello et al., 2020). Uncertainty for the threshold is derived by bootstrapping 1000 times the available data (see Papale et al., 2006). This procedure is executed for each year separately, resulting in a u_{*th} value and its uncertainty for each year. Here we estimate u_{*th} from both F_c and $F_c + S_c$ time series for each site and year.

The Ω threshold value for decoupling (Ω_{th}) and its uncertainty were estimated by bootstrapping the normalised F_c data 1000 times and evaluating the threshold with change point detection algorithm (Barr et al., 2013) from the bootstrapped data. In addition to this bootstrapping approach, the change point detection algorithm was used separately for each site and site-specific Ω_{th} values were estimated. The same was done also for the $F_c + S_c$ time series in order to verify the hypothesis that when S_c is added, the Ω threshold will be more variable and difficult to constrain due to the processes involved in the storage flux evolution that are not represented in the Ω formulation.

Matthews correlation coefficient (MCC) was used to evaluate the agreement between two binary time series of low turbulence flags (0=decoupled, 1=coupled) derived based on u_* and Ω thresholds (u_{*th} and Ω_{th} , respectively). MCC can be calculated as

$$MCC = \frac{(CC * DD) - (DC * CD)}{\sqrt{(CC + DC)(CC + CD)(DD + DC)(DD + CD)}}, \quad (5)$$

where CC , DD , CD and DC are the amounts of data in “Coupled-Coupled”, “Decoupled-Decoupled”, “Coupled-Decoupled” and “Decoupled-Coupled” groups, respectively. “Coupled-Coupled” group relates to periods which both Ω_{th} and u_{*th} categorise as coupled, “Decoupled-Decoupled” relates to periods which both metrics categorise as decoupled and in “Coupled-Decoupled” and “Decoupled-Coupled” groups the two metrics disagree. See Fig. 2 for an example how the thresholds delineate data into these four groups. $MCC=+1$ means that there is complete agreement between the two binary low turbulence flags ($DC = 0$ and $CD = 0$), $MCC=0$ means that there is no relation between the flags, i.e. same amount of data in all of the four groups, and $MCC=-1$ means complete disagreement between the flags ($CC = 0$ and $DD = 0$). Hence MCC is essentially a correlation coefficient between the two binary time series. For comparing u_* and Ω based low turbulence flags, MCC was calculated between low turbulence flags derived using fixed Ω_{th} and all the possible u_{*th} values at each site.

Two-sample Kolmogorov-Smirnov test was used to evaluate whether the flux ($F_c + S_c$) data distributions after Ω filtering with a fixed threshold or u_* filtering with site-specific threshold came from the same probability distribution. This analysis was done separately for daytime and night time flux data.

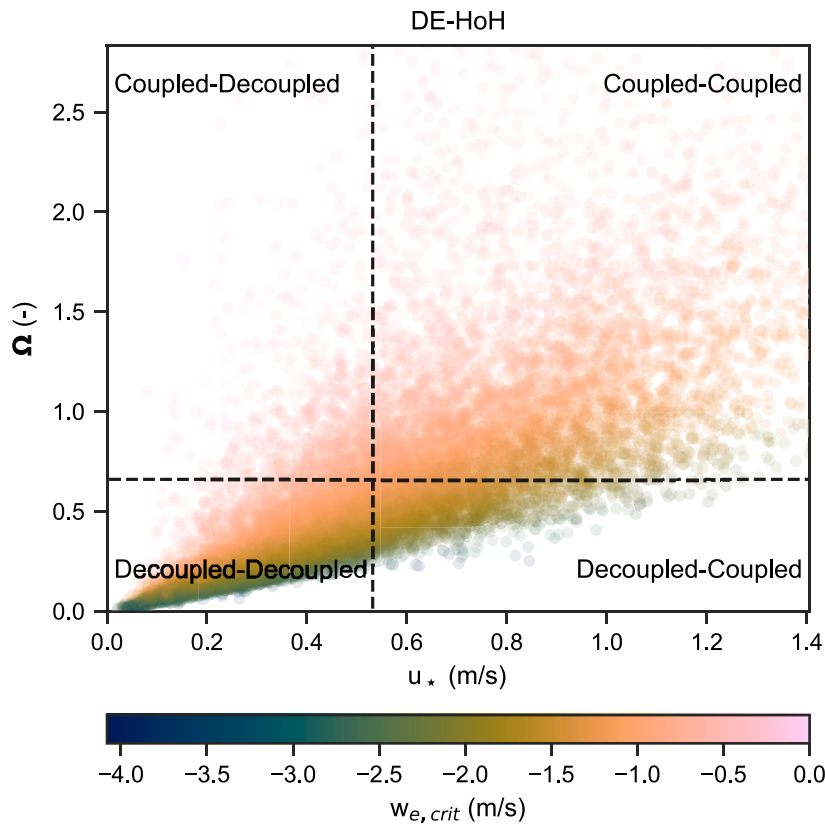


Fig. 2. Agreement between Ω and u_* at DE-HoH. Ω and u_* (derived using F_c) thresholds shown with black dashed lines delineate the data into four groups (Decoupled–Decoupled, Decoupled–Coupled, Coupled–Coupled and Coupled–Decoupled) which are used to calculate MCC (see Section 2.2). Note that data with specific u_* value can correspond to either coupled or decoupled regime depending on $w_{e,crit}$ (i.e. hindrance for coupling).

3. Results and discussion

This section includes analyzes of night time CO₂ fluxes against different metrics for flow decoupling, comparisons between the metrics, analysis on the processes controlling decoupling and the effect of filtering flux time series based on the different metrics on the flux data distributions.

3.1. Analyzing night time fluxes against different metrics for flow decoupling

Fig. 3 shows normalised nighttime F_c plotted against u_* , σ_w and Ω . This kind of analysis views the decoupling from fluid dynamics perspective, i.e. vertical turbulent flux is evaluated against metrics for vertical turbulent mixing. u_* and σ_w dependencies are similar (Figs. 3a and 3b) which could have been expected since u_* and σ_w are strongly correlated (e.g. Kaimal and Finnigan, 1994) albeit representing different facets of the flow. This suggests that they both perform equally well in identifying low turbulence periods (but see Acevedo et al. (2009), Jocher et al. (2017)). Different sites show different u_* (σ_w) thresholds and also otherwise the dependencies between normalised F_c and u_* (or σ_w) vary between sites. Generally, u_* (σ_w) thresholds increased with measurement height (Fig. 3a and 3b) in accordance with prior literature (e.g. Pastorello et al., 2020). All these findings are consistent with prior literature and confirm the fact that the definition of a u_* (or σ_w) threshold must be done for each site and a single value valid for all conditions cannot be used.

In contrast, the sites show more similar behavior when normalised F_c is plotted against Ω (Fig. 3c). Normalised F_c plateau roughly when $\Omega > \Omega_{th}$ with similar Ω_{th} value at all sites (Peltola et al., 2021b). However, when the Ω_{th} values are estimated separately for each site from F_c (circles in Fig. 5), variability across sites does exist but there

is no systematic pattern akin to the one observed with u_* or σ_w , e.g. threshold value increased with height. It can be speculated that the cross-site variability in Fig. 3c and between the circles in Fig. 5 is related to the uncertainty and assumptions made in the calculation and derivation of Ω , uncertainty in F_c normalisation and to the stochastic nature of turbulent flow. In particular, the canopy drag term in $w_{e,crit}$ is uncertain due to several assumptions made in the derivation. For instance, canopy density was assumed constant with height when deriving Ω and this is typically a poor assumption in deciduous or pine forests. However, $w_{e,crit}$ integrates canopy drag over the whole vertical column which may partly remedy the inaccuracy stemming from this assumption. In addition, vertical wind speed fluctuations are likely differently distributed at different sites, i.e. above-canopy flows are typically dominated by sweeps (e.g. Brunet, 2020) whereas flows above smoother surfaces are more evenly balanced between sweeps and ejections. Hence at canopy flows smaller Ω value might suffice for coupling. Nevertheless, we argue that these uncertainties do not prevent meaningful analyzes to be made with Ω and stress that the sites ranged from agricultural grasslands ($z_{EC}=3$ m, FI-Jok) to dense and tall forests ($z_{EC}=38$ m and one-sided PAI=9.4 m² m⁻², US-MRF) and they all show similar Ω dependence. This suggests that despite uncertainties Ω captured the dominant features of decoupling.

Violinplot in Fig. 3c shows the distribution of the Ω_{th} values obtained with bootstrapping. The distribution is slightly skewed to the right (skewness=0.52), but values are closely centered around the mean (mean=0.66, standard deviation=0.06). This value for the threshold ($\Omega_{th}=0.66$) is slightly higher than the one derived heuristically in Peltola et al. (2021b). Site-specific Ω_{th} values derived from F_c agree with these statistics obtained with bootstrapping (Fig. 5).

Note that the change in storage term (S_c) was not included in the analysis above. When included, the scatter between sites increased and a common dependence was not as evident when plotted against Ω

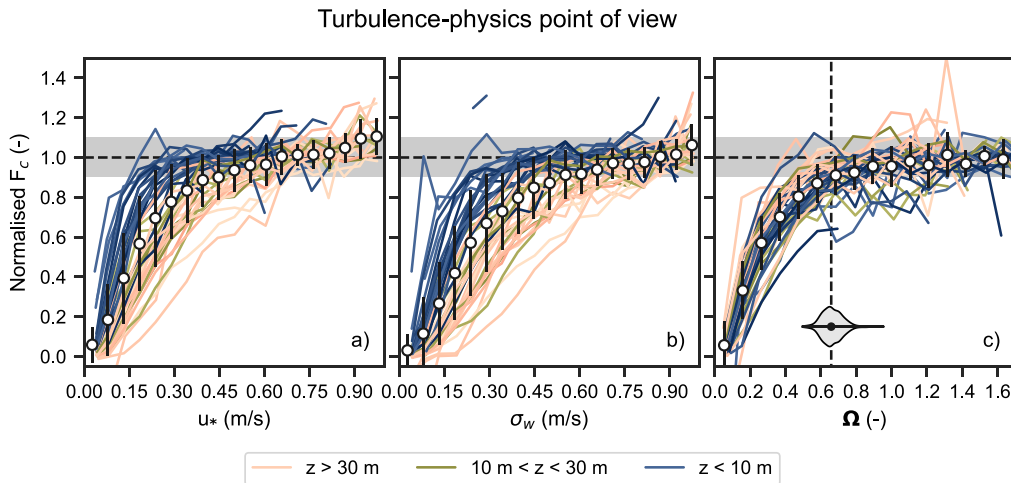


Fig. 3. Bin medians of normalised night time F_c against different metrics for flow decoupling. Here the flow decoupling is analyzed from fluid dynamics perspective, i.e. turbulent flux is analyzed against metrics for turbulent mixing strength. Medians for bins with more than 30 data points were plotted. Nighttime data from days when daily mean air temperature was above 5 °C were used. Each curve corresponds to a specific site and colors were defined based on three EC measurement height bins and unique shade of color for each site. Circles (errorbars) denote means (standard deviation) over all the sites. Subplot c: horizontal violinplot shows the distribution of Ω_{th} values obtained by utilising change-point detection algorithm (Barr et al., 2013) on bootstrapped data and vertical dashed line shows the universal value for Ω_{th} . It should be noted that the comparison of u_* against F_c does not strictly follow standard procedures of e.g. ICOS.

(compare Figs. 4c and 3c). Furthermore, the Ω_{th} values estimated from $F_c + S_c$ time series separately for each site show pronounced scatter, especially for tall tower sites (Fig. 5). This kind of analysis of $F_c + S_c$ concurs with the flux measurement community standard practices using u_* where night time $F_c + S_c$ is analyzed against u_* (Pastorello et al., 2020) and in general to the biological standpoint on decoupling in which the best available estimate for nocturnal respiration is analyzed against turbulence metrics. We hypothesise that the lack of universal Ω threshold when analyzed against $F_c + S_c$ might be due to the possibility that at some sites the flux underestimation at low Ω ($\Omega < \Omega_{th}$) was caused by storage of respired CO₂ close to the ground, and hence captured by S_c , whereas at others transport via advection (F_{res}) was more important and hence not captured by S_c . The importance of S_c versus F_{res} at each site likely depends on local conditions, such as local topography and surface heterogeneity. Interestingly, the difference between site-specific Ω_{th} values estimated from F_c and $F_c + S_c$ was large especially at tall tower sites indicative that at these locations S_c was an important component of the mass balance (Eq. (1)) during low vertical mixing ($\Omega < \Omega_{th}$).

Fig. 6 summarises these findings and we delineate three regimes: regime 1 where F_c dominates the mass balance ($\Omega > \Omega_{th}$ and $NEE \approx F_c$), regime 2 where S_c is also important ($NEE \approx F_c + S_c$) and regime 3 where F_{res} makes a significant contribution to mass balance ($NEE \approx F_c + S_c + F_{res}$). For the rest of the study we assume that a universal value for Ω_{th} applies with value 0.66 meaning that regime 1 can be estimated without site-specific thresholds. However, the results indicate that similar universal Ω threshold cannot be delineated for the approximation $NEE \approx F_c + S_c$, in other words transition between regimes 2 and 3 depends on local site characteristics. Ω is a metric for vertical turbulent mixing and as such is not able to distinguish which mass balance terms (S_c or F_{res}) would explain the flux underestimation during low mixing.

Deriving a globally unified metric for identifying when $NEE \approx F_c + S_c$ is valid is likely very difficult as the metric would need to combine at least two different aspects: processes controlling vertical turbulent mixing (related to F_c) and processes controlling the storage (i.e. S_c). S_c is significant only in the absence of processes that transport gases, advective or turbulent, and hence the variability of S_c is controlled by both vertical and horizontal transport processes. Therefore, the ideal metric for identifying periods where $NEE \approx F_c + S_c$ is valid should encompass all these transport processes, in essence it should describe

the whole mass balance (Eq. (1)). However, this has proven to be very difficult task in the past studies, as the scientific understanding on gas transport processes is still undeveloped.

One should also note that S_c is almost always estimated from single tower measurements and such estimates will always be biased as spatiotemporal gas concentration observations would be needed for accurate S_c estimation (Finnigan, 2006). As such spatiotemporal observations are very demanding, protocols aiming at maximising the accuracy of single tower S_c estimates have been developed (Montagnani et al., 2018; Xu et al., 2019) but not always followed outside standardised measurement networks. Therefore for the time being it might be prudent to utilise metrics (e.g. Ω) that identify periods when $NEE \approx F_c$, assign higher degree of trust on those periods in all the further flux data analyzes (based on either $F_c + S_c$ or F_c) and treat periods where S_c is high relative to F_c with extreme caution.

3.2. Comparison between Ω and u_*

While u_* and σ_w represent different facets of the flow, i.e. vertical turbulent momentum flux and vertical turbulent kinetic energy, respectively, they are still strongly correlated (Kaimal and Finnigan, 1994) and this correlation induces also a correlation between u_* and Ω (Fig. 2). If we assume that Ω describes the physics behind the decoupling accurately, then this correlation explains the relative success of using u_* as a low turbulence filtering metric. However, there is scatter between Ω and u_* (Fig. 2), especially at tall tower forested sites, indicating that the flow can be coupled or decoupled (based on Ω) at specific u_* value depending on $w_{e,crit}$. At low u_* , the flow is almost always decoupled, at mediocre u_* flow can be coupled or decoupled depending on $w_{e,crit}$ and at high u_* flow is almost always coupled (see Fig. 2). This means that when night time CO₂ fluxes are analyzed as a function of u_* a gradual dependence of CO₂ fluxes on u_* can emerge, simply due to the fact that decoupled and coupled periods are mixed to varying degree in the analysis and respiration is underestimated during decoupling but estimated accurately during coupling. This might partly explain why at some EC sites a clear u_* threshold is not observed and the CO₂ fluxes increase gradually as a function of u_* , but this common finding is likely also related to F_{res} . This behavior can be seen also in Fig. 3a and 4a. At tall tower sites normalised fluxes increase gradually as a function of u_* or σ_w , whereas at short tower sites more clean-cut u_* threshold can be observed. In contrast, dependence on Ω is more similar across all sites.

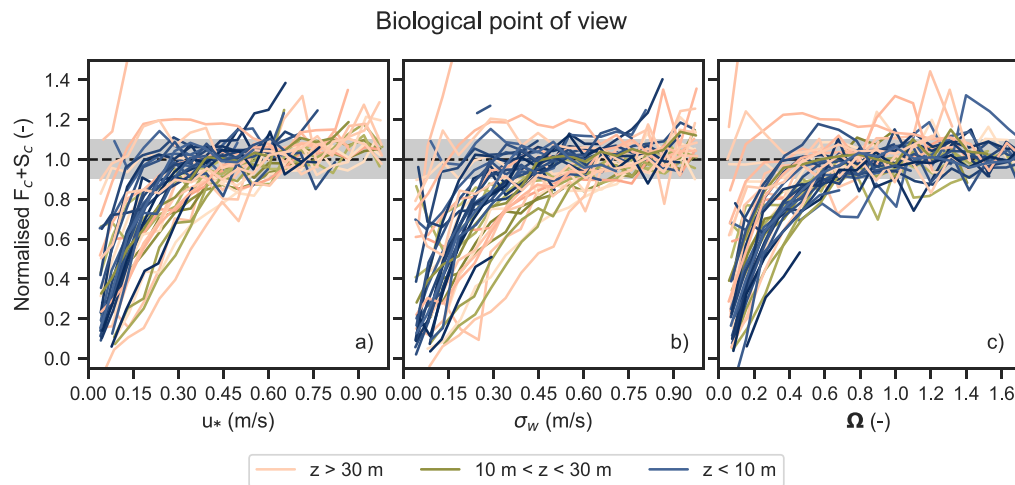


Fig. 4. Same as Fig. 3 but for $F_c + S_c$. Here the problem of decoupling is analyzed from biological perspective, i.e. by analyzing the best estimate for ecosystem respiration ($F_c + S_c$) against different turbulence metrics. Line colors follow Fig. 3.

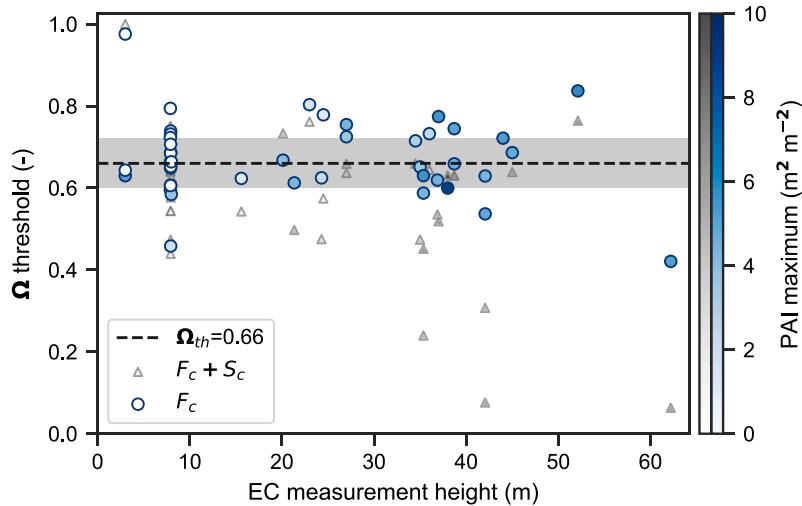


Fig. 5. Site-specific Ω thresholds estimated separately from F_c and $F_c + S_c$ time series for each site plotted against EC measurement height. Horizontal dashed line and gray area depict the universal value for Ω threshold and its uncertainty band of one standard deviation, respectively. Blue and gray colors refer to maximum PAI value observed at each site. Note that the site-specific thresholds estimated from F_c time series vary around the universal value, whereas thresholds estimated from $F_c + S_c$ time series depart from it and show more scatter.

The MCC values obtained by comparing u_{*th} based flagging and Ω_{th} based flagging with a fixed value (0.66) showed a distinct maxima at a certain u_{*th} value, specific to each site (Fig. 7a). The MCC values do not reach +1, i.e. perfect agreement between the flags, at any u_{*th} value indicating that there is a fundamental difference between Ω and u_* based low turbulence flagging and the two metrics flag partly different periods. In addition, the peak MCC values decrease with increasing EC measurement height and canopy density indicating that the difference between u_* based and Ω based low turbulence flagging increases. For instance, the site with very thick and tall canopy (PAI=9.4 $m^2 m^{-2}$, US-MRF, Thomas et al. (2013)) and hence strong canopy drag has a peak MCC of only 0.14 (Fig. 7a). These findings reflect the fact that u_* filtering does not consider temporal changes in forces hindering the coupling below the measurement height which in contrast are reflected in $w_{e,crit}$ and hence in Ω . While not shown, similar results apply when comparing σ_w and Ω based low turbulence filtering, since σ_w and u_* are strongly correlated and follow $\sigma_w \approx 1.25u_*$ over a wide range of stabilities and ecosystem types.

The u_{*th} values derived from the location of peak MCC were correlated ($r=0.70$) with u_* thresholds derived from F_c independently with the tool implemented in the ONEflux software package (Pastorello

et al., 2020) (Fig. 7b). This indicates that Ω explains the bulk of the variability of u_* thresholds observed across sites (e.g. Papale et al., 2006; Barr et al., 2013; Pastorello et al., 2020) when estimating u_{*th} from F_c . To date, clear quantitative explanation for the u_{*th} variability across sites has been lacking (Barr et al., 2013), while the variability has been qualitatively explained in prior studies (e.g. Pastorello et al., 2020).

3.3. Drivers of flow decoupling and surface flux underestimation

The similar Ω threshold at all sites can be considered as an indicator of the fact that once vertical turbulence was strongly enough coupled with the ground, the contribution of F_c to the mass balance (Eq. (1)) did not anymore change and that Ω was an appropriate metric for this coupling. This however does not necessarily mean that under strong coupling F_c is an accurate estimate of the ecosystem exchange since the above analyzes are ignorant of such contribution of e.g. advection to the mass balance that does not correlate with Ω . This might include for instance the modulation of turbulent flux via advection caused by topography induced re-circulation regions (Katul et al., 2006; Poggi and Katul, 2007; Ross, 2011; Ross and Harman, 2015; Chen et al., 2019) or

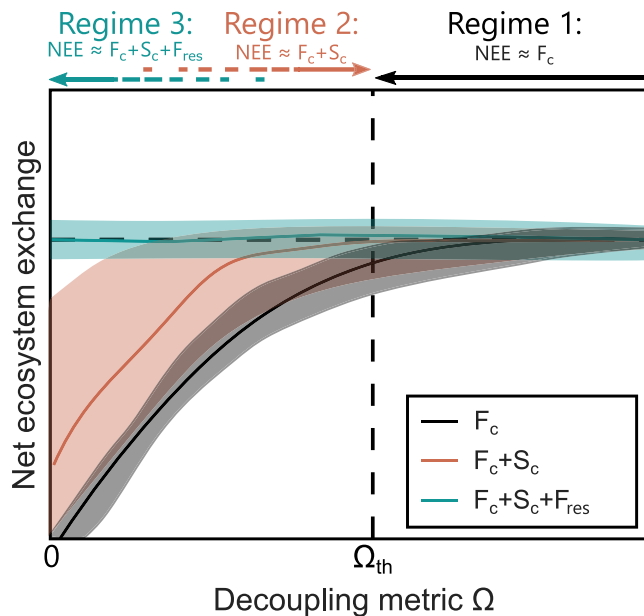


Fig. 6. Schematic figure showing the importance of different mass balance terms as a function of Ω . Shaded areas show approximate variability across sites and lines the typical dependency. Three regimes are identified based on Ω and different mass balance terms are important in these regimes (see Section 3.1). Universal value for Ω_{th} is assumed to delineate regime 1, whereas transitioning between regimes 2 and 3 depend on local site characteristics.

surface roughness discontinuities such as forest edges (Kanani-Sühring and Raasch, 2015, 2017; Ma et al., 2020). Ω is simply uninformed of such two dimensional flow interactions induced by surface heterogeneities as it measures only the vertical coupling and the same applies to e.g. u_* and σ_w . Nevertheless, Ω was able to delineate the periods during which vertical turbulent transfer was an important contribution to the mass balance. Hence, it can be inversely used to evaluate periods and/or locations at which the contribution of F_c to the mass balance decreases and the importance of the other terms in the mass balance increase.

In order to evaluate the effect of stability on decoupling, Ω dependency on Monin–Obukhov stability parameter (ζ) was analyzed (Fig. 8). Ω decreased with ζ and fell below the approximate threshold for coupling (Ω_{th}) when $\zeta > 0.02\text{--}0.3$, depending on site. Short tower sites ($z_{EC} < 10$ m) without pronounced canopy showed similar ζ threshold for coupling (0.15...0.3). This threshold is in the same range where Mahrt et al. (1998) found flow to decouple from the surface and Li et al. (2016) found the size of dominant momentum transporting eddies (Ozmidov length scale) to fall below z_{EC} , indicating that turbulent flow detached from the surface.

For flux measurements above forests, similar widely applicable ζ threshold could not be found (Fig. 8). We take this as an indicator for the fact that above-canopy ζ is a poor predictor for cross-canopy coupling since it does not directly relate to below-canopy stratification (Belcher et al., 2008; van Gorsel et al., 2011) and misses the influence of drag on coupling.

Drag force hindering coupling increased with PAI and hence $|w_{e,crit}|$ increased and the increase was stronger than the co-occurring increase in σ_w (Fig. 9). Hence, in near-neutral situations Ω and the cross-canopy coupling at the forested sites was related to PAI and L_c/h (Eq. (B.2)) as shown in prior studies (Belcher et al., 2003; Nepf et al., 2007; Ghisalberti, 2009; Harman and Finnigan, 2007, 2008; Cava et al., 2008). At the very dense forest site (US-MRF, PAI=9.4 m² m⁻²) σ_w was lower than at sites with sparser canopies (see Fig. 9), likely due to tightly closed canopy at this forest site which suppressed the generation of canopy eddies at the canopy height (Brunet, 2020) and

hence decreased σ_w . The σ_w values show a broad maximum at PAI ≈ 3 m² m⁻² in Fig. 9. The maximum can be explained as follows: at lower PAI surface roughness and hence turbulence generation increases with PAI, whereas at higher PAI the canopy gets more closed, surface is less rough and hence turbulence generation is weaker.

Brunet (2020) argued that beyond an undefined PAI value, which they approximate to be greater than 5 m² m⁻², the above-canopy flow is almost fully decoupled from the canopy sublayer. Our results in Fig. 9 are broadly in line with this argument and suggest that when PAI is roughly above 4...5 m² m⁻² subcanopy air layer is decoupled from the above canopy flow also in near-neutral situations (in these situations σ_w is below 0.66| $w_{e,crit}|$). Another estimate for this limit can be acquired by using Eq. (B.2) and assuming a representative vertical turbulent intensity σ_w/U_h of 0.35, which results to the finding that the flow decouples from the surface in neutral conditions when PAI ≈ 4.8 m² m⁻². These results suggest that above dense forest canopies (i.e. low L_c/h or high PAI) decoupling is frequent and F_c alone rarely represents ecosystem exchange. See Thomas et al. (2013) for one practical approach how to overcome this issue by utilising multi-layer EC measurements.

Besides stability and canopy density, also EC measurement height had an impact on the occurrence of decoupling. The average night time $|w_{e,crit}|$ increased with EC height, indicative that stronger downdrafts (i.e. higher σ_w) were needed in order to couple with the ground (Fig. 10). However, σ_w did not show similar increase suggesting that occurrence of flow decoupling increased with the EC measurement height (Peltola et al., 2021b). The increase of $|w_{e,crit}|$ with height was due to thicker stable layer below EC height but also due to higher canopy drag at sites with tall towers (short towers were mostly in open terrain). We conclude based on this that EC flux measurements with short towers are likely less affected by flux underestimation during low turbulence.

For exemplifying how Ω can be used to diagnose decoupling at specific sites, Fig. 11 shows the timing of decoupled and coupled periods as identified with Ω at two forest sites: evergreen needleleaf boreal pine forest (FI-Hyy, Fig. 11a) and deciduous broadleaf temperate forest (US-xSE, Fig. 11b). The seasonally varying PAI at the broadleaf forest had a marked effect on seasonality of coupling at the site (Fig. 11b). During leafless period with low PAI the above-canopy flow was almost always coupled with the forest floor during daytime, but after leaf unfolding during spring and resulting increase in PAI the canopy closed and the above-canopy flow decoupled from the forest floor almost permanently. PAI varied seasonally between 0.6 and 5.6 m² m⁻² at this site. Below-canopy stratification was slightly stable during daytime when PAI was high, likely due to solar radiation heating the canopy, but not the forest floor. In contrast, at the evergreen boreal pine forest the above-canopy flow was almost always coupled with the forest floor during daytime and decoupling took place primarily at night (Fig. 11), although it took several hours after the sunrise for the flow to couple with the forest floor during summer mornings. This was likely due to low elevation angle of the Sun at these high latitudes which meant that the Sun was heating the canopy, but not the forest floor during these morning hours. The forest at FI-Hyy was thinned during the winter 2019–2020 which decreased the PAI from 3.6 to 2.1 m² m⁻², and basal area by ca. 30% (Aslan et al., 2024) and this is also reflected in the results in Fig. 11a which show lower impact of canopy drag on decoupling during the year 2020 due to the lower PAI. This kind of diagnoses of reasons behind decoupling are not possible with the more traditional decoupling metrics, such as u_* and σ_w .

3.4. Impact of low turbulence filtering on data coverage and flux data distributions

Low turbulence filtering of flux time series based on Ω removed more data points from the flux time series than based on u_* filtering with u_{*th} derived from $F_c + S_c$ using ONEflux, especially during daytime at tall towers (Fig. 12a) and night time irrespective of the tower

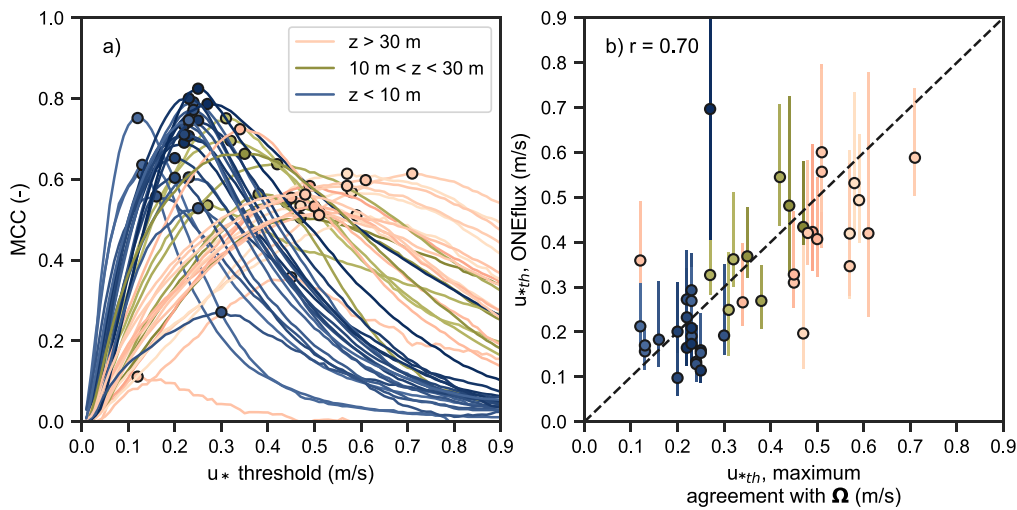


Fig. 7. (a) MCC calculated for each site between low turbulence flags based on Ω with a fixed threshold and u_* with a range of threshold values. (b) Comparison of u_* thresholds determined with ONEflux (using F_c) with u_* threshold derived from the MCC curve peak (subplot a). Errorbars show the uncertainty of u_* threshold derived with ONEflux (10th and 90th percentiles of the values obtained with bootstrapping, see Pastorello et al. (2020)). Dashed line shows the 1:1 line. r =Pearson correlation coefficient. Line colors follow Fig. 3.

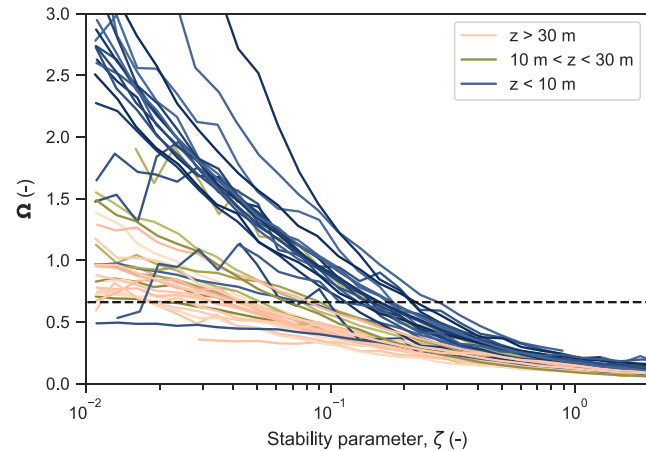


Fig. 8. Bin medians of Ω plotted against Monin–Obukhov stability parameter ζ . Horizontal dashed line shows the Ω threshold for coupling. Line colors follow Fig. 3.

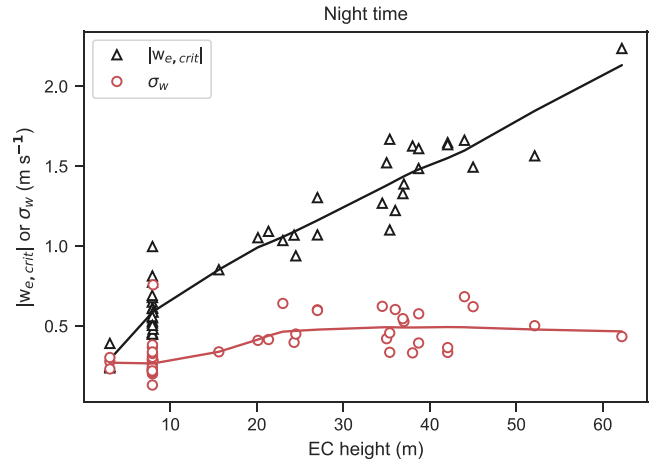


Fig. 10. Site average values of σ_w and $|w_{e,crit}|$ observed during night time plotted against EC measurement height. Lines show lowess fits for guiding the eye.

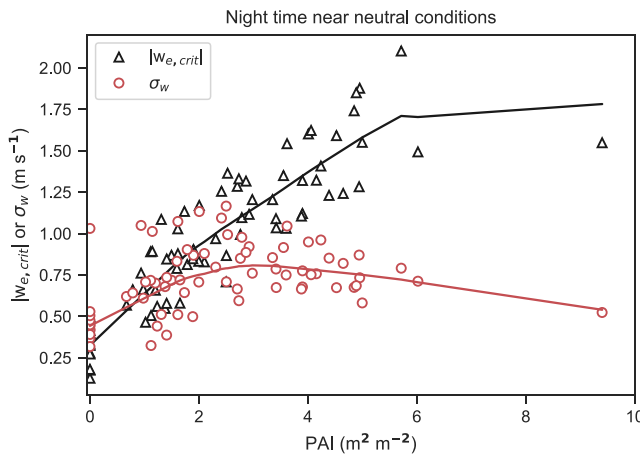


Fig. 9. Average values of σ_w and $|w_{e,crit}|$ observed during night time near neutral conditions ($|\zeta| < 0.05$) plotted against PAI. Data from sites with varying PAI, e.g. deciduous forests, were separated to low, medium and high PAI categories based on first and third quartiles of site PAI data prior averaging and plotting. Lines show lowess fits for guiding the eye.

height (Fig. 12b). The higher data filtering percentage for Ω was to be expected since it derives the regime where $NEE \approx F_c$, whereas u_{*th} estimated from $F_c + S_c$ derive the regime where $NEE \approx F_c + S_c$ is valid and typically these periods are more common. There was a strong variability across sites as shown by the scatter in Fig. 12, which indicate that amount of data filtered is not solely dictated by the EC height but is related also to local conditions, such as canopy density and typical strength of nocturnal stable stratification. For instance, sites with soils that have low heat capacity, hence are susceptible for strong nocturnal cooling, or are located in depressions, hence are susceptible for nocturnal cold air pooling, may exhibit stronger nocturnal air stratification and as a consequence have higher $|w_{e,crit}|$ and lower Ω . This results in more data from these sites to be filtered out. Accordingly, high amount of filtered data increases the need for flux time series gapfilling and hence increases the uncertainty of carbon balance estimates.

One way to differentiate the performance of decoupling filtering methods is to compare the carbon balances (Stiegler et al., 2023). However, this would introduce additional uncertainty to the analysis due to site-dependent gap distribution which is a result of many additional external factors (e.g., spikes, data logging, power cuts, instrument malfunction and maintenance history etc.), affecting the accuracy of

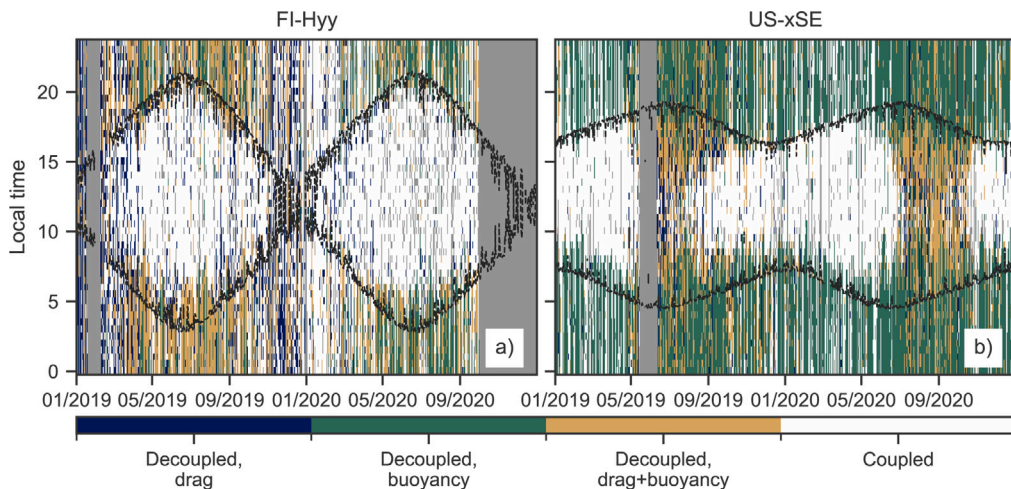


Fig. 11. Timing of coupled ($\Omega > \Omega_{th}$) and decoupled ($\Omega < \Omega_{th}$) periods at two example sites during two years: (a) evergreen needleleaf forest FI-Hyy, and (b) broadleaf deciduous forest US-xSE. The dominant hindering force causing decoupling was evaluated by calculating $w_{e,crit}$ with neglecting either buoyancy or canopy drag in Eq. (2) and then estimating how big fraction these simplified $w_{e,crit}$ were from the full $w_{e,crit}$ (using arbitrary limit of 0.8). Black dashed lines highlight sunset and rise (global radiation equal to 10 W m^{-2}). Gray areas show missing data.

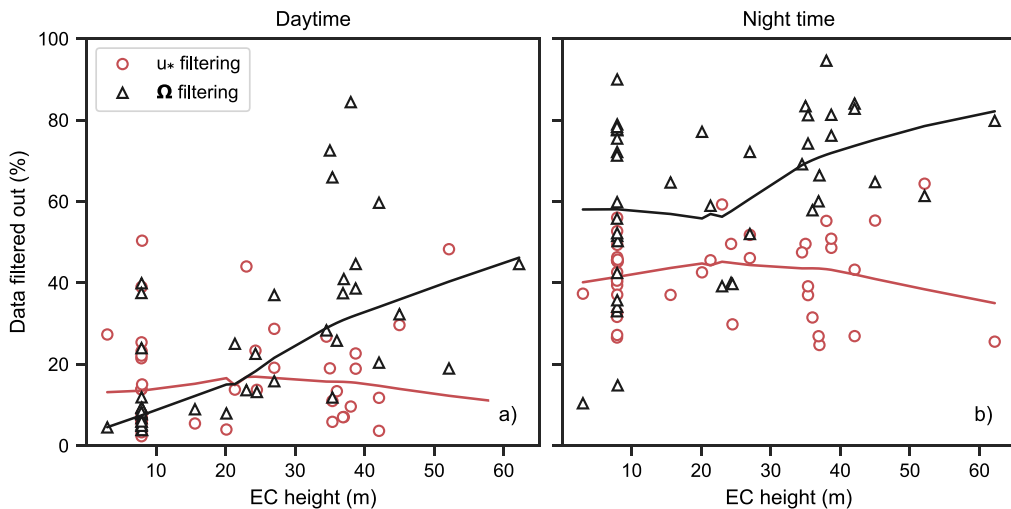


Fig. 12. Amount of data filtered based on fixed Ω threshold and site-specific u_* threshold estimated with ONEflux from $F_c + S_c$ (see Section 3.1) as a function of EC measurement height. Only periods when both metrics (Ω and u_*) were available were considered. Night time was estimated as periods when global radiation was below 10 W m^{-2} and daytime when it was above 10 W m^{-2} .

gap-filling methodologies, hence cannot solely reflect the performance of decoupling filtering methods. Instead, we evaluate the impact of low turbulence filtering on flux data ($F_c + S_c$) distributions, see Figs. 13 and 14. 42 sites were available for this analysis. By using Kolmogorov-Smirnov test, at 29 out of 42 sites for night time and at 26 sites for daytime we could reject ($p < 0.05$) the null hypothesis that the sample distributions came from the same distribution, i.e. at these sites the filtering resulted in different distributions for the flux data.

While Kolmogorov-Smirnov test identified differences, the differences between mean night time and daytime fluxes after filtering with Ω or u_* were small and below 15% of the site mean flux at 32 sites during day and at 29 sites during night time. There was no clear indication that either of the two filtering metrics would systematically result in higher fluxes, but the differences between site means after filtering varied around zero. Impact on flux data spread, as measured with difference between standard deviations of flux data after filtering, was not high during the day (absolute relative difference between spread estimates was below 10% at 37 sites), but the spread estimates varied slightly more during night time (absolute relative difference between the estimates was below 15% at 29 sites). Ω filtering resulted

in a smaller spread of night time data at most of the sites (31 sites), indicative that the night time flux data were less variable after Ω filtering than after u_* filtering. These findings can also be seen in the distributions shown in Figs. 13 and 14. Especially at tall tower sites with marked seasonality in PAI (e.g. US-xST, US-xBR, US-xUN, FR-Fon, US-xRN, US-xDL, DE-HoH, US-xSE), the flux data distributions after Ω filtering were more peaked, showed smaller spread and were less skewed to the right for night time and skewed to the left for daytime data, respectively. Further scrutiny on the data suggested that this was caused by the finding that Ω retained more data from periods when PAI was low, i.e. outside growing season with low fluxes, and filtered more strictly periods when PAI was high, i.e. growing season with high fluxes, due to the dense canopy hindering vertical exchange (see Fig. 11b for an example). Similar seasonally varying filtering was not observed when using u_* as a filtering metric as u_* filtering was executed with a constant threshold value for each site and this discrepancy between filtering caused the differences between flux distributions.

The found differences in the flux data distributions will have an effect on flux time series gapfilling, since the gapfilling algorithms will then have different data at their disposal. Hence carbon balance estimates will be affected by the choice of using Ω or u_* for low turbulence

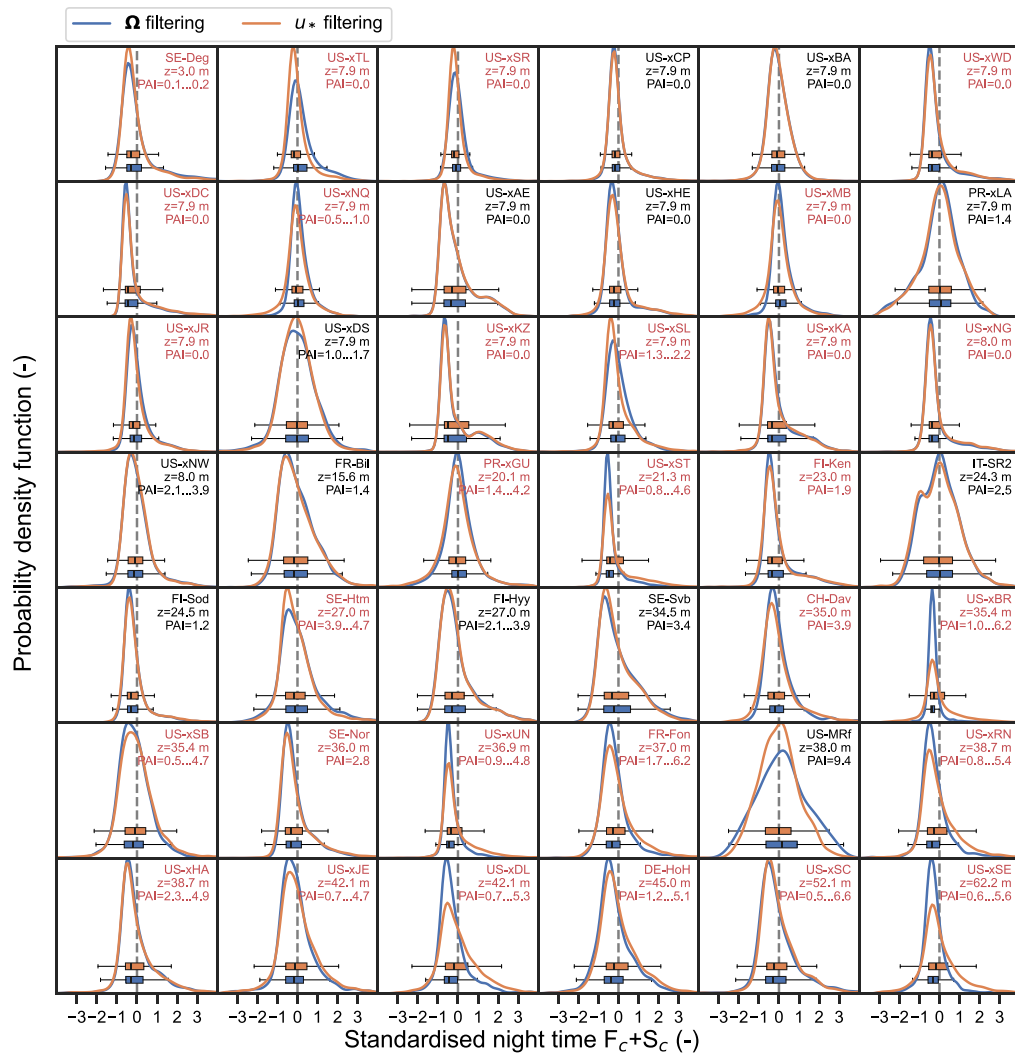


Fig. 13. Distributions of night time $F_c + S_c$ values after filtering based on u_* and ONEflux thresholds derived from $F_c + S_c$ and on Ω and universal threshold at each site. Distributions were estimated with kernel-density estimates using Gaussian kernels (lines) and also via boxplots for each site. Text in the subplots is red for such sites for which the Kolmogorov-Smirnov test identified the distributions to be different ($p < 0.05$). Values were standardised ((x -mean)/std) with mean and standard deviation calculated from u_* filtered data before analysis.

filtering, especially if there is seasonality in the amount of filtered data. However, uncertainties related to gapfilling algorithms themselves will likely dominate the uncertainty of annual carbon balances. Therefore, the selection of using either Ω , u_* , σ_w or some other metric for filtering low turbulence periods from the EC data should not be motivated by the effort of obtaining more accurate annual carbon balance estimates, but rather by the effort of trying to utilise scientifically sound and robust techniques that are ideally based on robust physical principles. With such techniques there is a clear defensible physical reasoning for discarding and retaining flux data. Besides its physics-based derivation, the added value of Ω comes from the fact that all the sites showed similar threshold for identifying when $NEE \approx F_c$ is valid. This will help in constraining the flow regimes without error prone estimation of site-specific thresholds.

4. Conclusions

By using eddy covariance (EC) data from 45 contrasting sites spanning from dense forests to open landscapes, we confirmed the wide applicability of Ω (Peltola et al., 2021b) in detecting periods when the turbulent flow was decoupled from the underlying surface. Ω forms a solid physical basis for detecting decoupling and hence provides key insights on processes controlling the decoupling. Consequently, Ω was

able to explain bulk of the friction velocity (u_*) threshold variability observed across sites.

Based on Ω , decoupling is driven by the strength of vertical turbulent mixing, static stability below EC height, measurement height above ground and in forested areas also by canopy density and turbulence intensity at the canopy height. These findings lead us to conclude that EC measurements at tall towers and/or above dense canopies are more prone to underestimate ecosystem gas exchange (at least at night) than measurements at shorter towers. Hence night time EC measurements from tall towers especially in forests should be analyzed very carefully when ecosystem gas (e.g. carbon dioxide) exchange is the target since flow above dense forests (PAI roughly above 4...5 $m^2 m^{-2}$) can be decoupled from the subcanopy gas exchange also in daytime near-neutral situations. In these conditions it could be also critical to correctly estimate the storage fluxes using an appropriate and spatial representative vertical concentration profile (e.g. Nicolini et al., 2018) as turbulent fluxes alone rarely represent the ecosystem-atmosphere exchange. We contend that for short EC towers measuring above short vegetation, u_* filtering with a site-specific threshold may be a practical choice for detecting decoupling for instance if temperature profile is not being measured.

Ω filtering with the universal threshold can result in a low data coverage, especially at tall tower forest sites, since it retains only

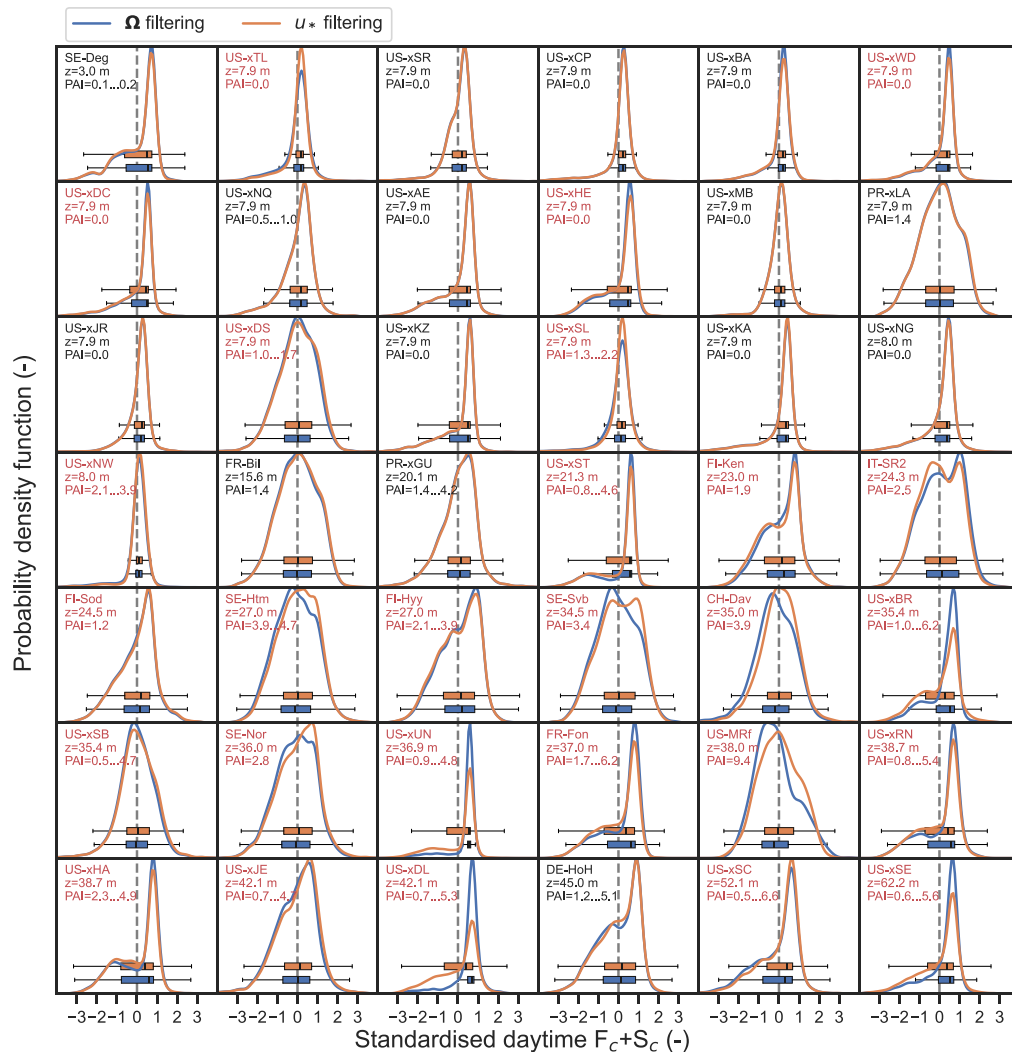


Fig. 14. Similar figure as Fig. 13 but for daytime data.

data points corresponding to periods when $NEE \approx F_c$. The low data coverage can be problematic when deriving e.g. annual carbon exchange. Hence an improved approach could be devised to identify periods when $NEE \approx F_c + S_c$ by using multiple constraints at the same time. The additional constraints should complement Ω by being able to identify periods when processes controlling the other mass balance terms, e.g. horizontal transport, are important and consider also the storage term when correctly measured. Ideally they should succinctly describe especially the processes controlling horizontal transport, since vertical turbulent transport is described with Ω . Since scientific understanding on these processes is still poorly developed, a combination of Ω and u_* might be a good practical starting point for devising such multiple constraints approach, also due to the long history on using u_* in this kind of analysis. The approach utilising both Ω and u_* would also provide a set of quality flags and indicators that identify the different regimes (see Fig. 6) in order to allow the data user to decide what to retain depending on the final data use.

In future work, Ω could also be cross-compared against intensive turbulence observations made at multiple towers with several measurement levels in the same forest in an effort to better constrain the processes, e.g. canopy drag, causing decoupling in canopy flows.

Finally, Ω showed similar decoupling threshold value at all the tested sites ($\Omega_{th} = 0.66 \pm 0.06$), despite slight scatter between sites which we attribute to the uncertainties of Ω calculation and data analysis approaches used in this study. Nevertheless, this suggests that Ω could

be used to evaluate the degree of coupling and to determine periods when $NEE \approx F_c$ holds at EC sites without site-specific thresholds, with the precondition that the needed measurements are in place which is the case in several standardised research infrastructures, e.g. ICOS and NEON. Accurate estimation of Ω requires standard EC equipment, temperature profile measurements below the EC height, and in forest sites plant area index (PAI) time series describing PAI variability at the site is needed as well. Put together, these findings can be considered as major improvements in our understanding on the reasons behind flow decoupling and low turbulence filtering of EC data and hence can guide more accurate analyzes of existing EC data and overall understanding of the turbulent flow observed at EC sites.

CRediT authorship contribution statement

Olli Peltola: Writing – review & editing, Writing – original draft, Visualization, Validation, Software, Project administration, Methodology, Funding acquisition, Formal analysis, Data curation, Conceptualization. **Toprak Aslan:** Writing – review & editing. **Mika Aurela:** Writing – review & editing, Data curation. **Annalea Lohila:** Writing – review & editing, Data curation. **Ivan Mammarella:** Writing – review & editing. **Dario Papale:** Writing – review & editing, Formal analysis. **Christoph K. Thomas:** Writing – review & editing, Data curation, Conceptualization. **Timo Vesala:** Writing – review & editing. **Tuomas Laurila:** Writing – review & editing, Supervision.

Declaration of competing interest

The authors declare the following financial interests/personal relationships which may be considered as potential competing interests: Olli Peltola reports financial support was provided by Research Council of Finland. Dario Papale reports financial support was provided by EU - Next Generation EU Mission 4 - Component 2. Timo Vesala, Mika Aurela, Annalea Lohila reports financial support was provided by Research Council of Finland. Timo Vesala, Mika Aurela, Annalea Lohila reports financial support was provided by Finnish Ministry of Transport and Communications. Ivan Mammarella reports financial support was provided by University of Helsinki. Ivan Mammarella reports financial support was provided by Research Council of Finland. Ivan Mammarella reports financial support was provided by Horizon Europe. Part of the editorial board of Agricultural and Forest Meteorology - Timo Vesala If there are other authors, they declare that they have no known competing financial interests or personal relationships that could have appeared to influence the work reported in this paper.

Acknowledgments

Olli Peltola acknowledges Research Council of Finland for funding (grant no. 315424, 354298). Dario Papale acknowledges the support of the EU - Next Generation EU Mission 4 - Component 2 - ITINERIS Project (ID IR0000032 - CUP B53C22002150006). Timo Vesala, Mika Aurela and Annalea Lohila acknowledge the ICOS Finland, which was funded by the Academy of Finland and the ministry of Transport and Communications. IM thanks the support of University of Helsinki supported this work via ICOS-HY; Research Council of Finland supported this work via project N-PERM (Grant No. 341348) and the EU Horizon Europe-Framework Programme for Research and Innovation (Grant No. 101056921-GreenFeedBack). We thank Beverly Law for US-MRF data. We thank ICOS PIs, ICOS-ETC and ICOS Carbon Portal for providing the data on the fluxes. The National Ecological Observatory Network is a program sponsored by the National Science Foundation and operated under cooperative agreement by Battelle. This material is based in part upon work supported by the National Science Foundation through the NEON Program. This study has been undertaken using data from GBOV “Ground Based Observation for Validation” (<https://gbov.land.copernicus.eu/dataaccessRM/>) founded by European Commission Joint Research Centre FWC932059, part of the Global Component of the European Union’s Copernicus Land Monitoring Service. GBOV products are developed and managed by ACRI-ST with the support from University College London, University of Leicester, University of Southampton, University of Valencia and Informus GmbH. We thank Courtney Meier and the NEON network for the measurements collected in the field and used to generate GBOV products. We thank Pasi Kolari for useful discussions related to gapfilling flux time series.

Code and data availability

Python codes and data needed for reproducing the results shown in this manuscript can be found in Zenodo (<https://doi.org/10.5281/zenodo.14259134>). Additionally, the codes are shared also via Github (https://github.com/OPeltola/EC_Omega_filtering). ICOS data persistent identifiers: CH-Dav (https://hdl.handle.net/11676/9PY7uZw_JdXy9WWpWgp45Ik5), DE-Hai (https://hdl.handle.net/11676/WiCY4SusnZoel1_SJugCrXDM), DE-HoH (https://hdl.handle.net/11676/hWDToPTdjCZlmQu3t_QmOBJC), FI-Hyy (https://hdl.handle.net/11676/Nn_zvmRQW4i7iq3U8D3jNCR0), FR-Aur (https://hdl.handle.net/11676/B1Ce9kHD_o-jBOQ1lpAGwK6o), FR-Bil (<https://hdl.handle.net/11676/J9dwIEpZs3JBIvsWI3VbRyHe>), FR-Fon (https://hdl.handle.net/11676/iAES_z8kPfTowb_K9OrD9J-w), IT-SR2 (https://hdl.handle.net/11676/xsn55wvnOdLD_ta5UE19v42M), SE-Deg (<https://hdl.handle.net/11676/Pyl6-HjdM0-zHaPhTYYHOBYz>), SE-Htm (<https://hdl.handle.net/11676/w4UsoD0iDfPg-IHHvPYBGgv>), SE-Nor (<https://hdl.handle.net/11676/14259134>).

Table A.2

Description of all mathematical symbols used in this study listed in the order of appearance.

Symbol	Description
NEE	Net ecosystem exchange
F_c	Vertical turbulent flux of gas
S_c	The change in storage term
$F_{hf, d}$	Horizontal turbulent flux divergence
$F_{had, v}$	Horizontal advection
$F_{vad, v}$	Vertical advection
F_{res}	Sum of $F_{hf, d}$, $F_{had, v}$ and $F_{vad, v}$
u_*	Friction velocity
u_{*th}	Friction velocity threshold
σ_w	Standard deviation of vertical wind speed component
Ω	Decoupling metric
h	Canopy height
$w_{e, crit}$	Minimum vertical speed required for the air parcel to reach the ground
γ	Parameter describing wind speed and air parcel speed profiles below h
c_d	Drag coefficient
PAI	One-sided plant area index
U_h	Mean wind speed at the canopy height
g	Acceleration due to gravity
θ	Potential temperature
θ_e	Potential temperature of downward moving air parcel
Ω_{th}	Ω threshold
ζ	Monin–Obukhov stability parameter
z_{EC}	EC measurement height
d	Displacement height
L	Obukhov length
U	Wind speed
ϕ_m	Stability scaling function
F_{ref}	Reference flux time series
MCC	Matthews correlation coefficient
L_c	Canopy adjustment length scale or penetration depth
L_B	Buoyancy length scale

1676/BtuSQuDRWOCeHouJDvViHUpo), SE-Svb (<https://hdl.handle.net/11676/QfqUnGlc6UY4Fb8bCdBQbjMB>). NEON data DOI: Bundled data products - eddy covariance (<https://doi.org/10.48443/2ms3-a333>) and digital hemispheric photos of plot vegetation (<https://doi.org/10.48443/x12v-n568>).

Appendix A. Mathematical symbols

See Table A.2

Appendix B. Relating Ω to different length scales

In locations without extensive canopy cover (e.g. short grass) canopy drag can be neglected and then Ω reduces to

$$\Omega = \frac{L_B}{\sqrt{2}z_{EC}}, \quad (B.1)$$

where L_B is buoyancy length scale (Mahrt, 1979; Moum, 1996; Sorbjan, 2006; Mahrt et al., 2012) calculated with the bulk θ gradient ($L_B = \frac{\sigma_w}{\sqrt{\frac{g}{\theta} \frac{\theta_e - \theta}{z_{EC}}}}$) and z_{EC} is EC measurement height. On the other hand, above canopies in neutral conditions (θ gradient ≈ 0), Ω reduces to

$$\Omega \approx \frac{1}{2\gamma} \frac{\sigma_w}{U_h} \frac{L_c}{h}, \quad (B.2)$$

where $L_c = \frac{h}{c_d \text{PAI}}$ is canopy adjustment or penetration depth often used as a measure for the depth of the air layer directly interacting with the above canopy flow (Nepf et al., 2007; Cava et al., 2008; Ghisalberti, 2009; Harman and Finnigan, 2007, 2008). Note that Ω should always be calculated based on Eqs. (2) and (3). Eqs. (B.1) and (B.2) are introduced only for showing the connection between Ω and different length scales (i.e. L_B and L_c) used in some prior studies.

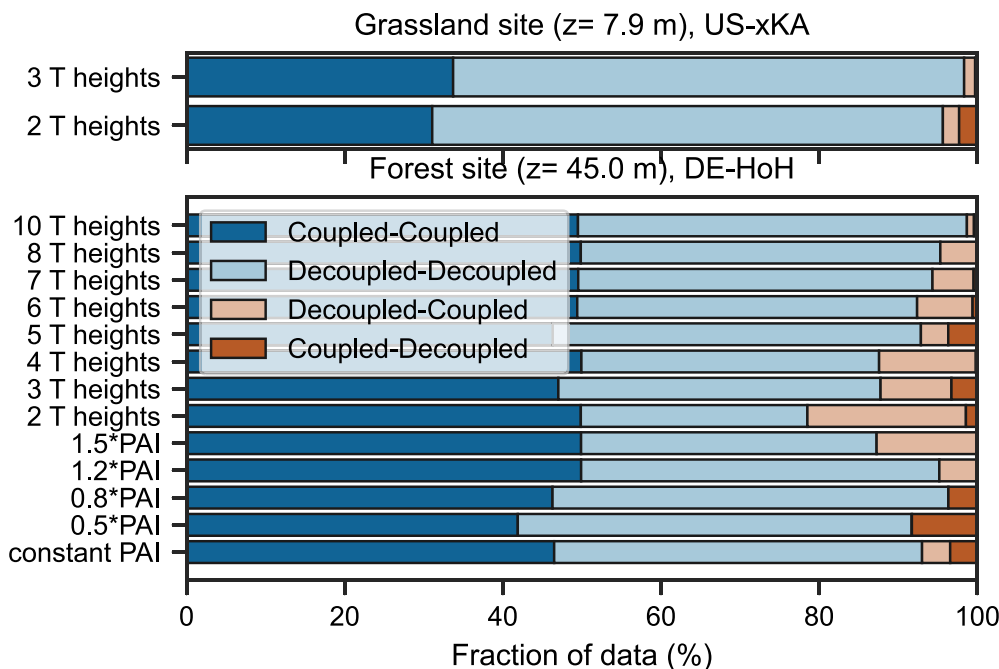


Fig. C.15. Sensitivity of Ω based low turbulence flagging on the accuracy of available PAI data and the amount of temperature measurement levels (T heights). Baseline estimates were obtained using all the available data and they were compared against flags estimated with reduced information. Coupled-Coupled=both flag as coupled; Decoupled-Decoupled=both flag as decoupled; Decoupled-Coupled=false identification of coupled regime; Coupled-Decoupled = false identification of decoupled regime.

Appendix C. Estimating the sensitivity of Ω to input variables

Estimation of the sources and magnitude of Ω uncertainty is important for evaluating the accuracy at which the flow decoupling can be determined with Ω , and for assessing the variables controlling the uncertainty. We evaluated the sensitivity of Ω calculation and Ω based low turbulence flagging and filtering on (1) accuracy of PAI data in forest ecosystems and (2) amount of temperature measurement heights below the EC measurement height. This was done for two contrasting measurement sites: tall deciduous forest with temporally varying PAI (DE-HoH) and open cropland (US-xKA). Both had detailed temperature profile measurements (four measurement levels at US-xKA and 13 at DE-HoH) and PAI data at DE-HoH enabling accurate Ω baseline estimation for sensitivity tests. Low turbulence flagging was not very sensitive to the accuracy of PAI data (Fig. C.15). With 20% error in PAI, the accuracy of low turbulence flagging was above 96% (sum of “Coupled-Coupled” and “Decoupled-Decoupled” fractions) and MCC was 0.93. With 50% error in PAI the accuracy and MCC were worse (90...93% and 0.81...0.87, respectively) and with constant PAI, the accuracy was 95% and MCC was 0.89. Hence, 20% errors in PAI are not critical when calculating Ω , however for capturing seasonality of decoupling due to plant phenology (seasonally varying PAI and hence canopy drag) PAI time series is needed.

The accuracy of low turbulence flagging increased when increasing temperature measurement heights used in Ω calculation (Fig. C.15). With seven temperature measurement heights an accuracy of 96% and MCC of 0.92 was reached at the forest site (DE-HoH). At the cropland site with relatively short tower (US-xKA) only two measurement heights were sufficient for reaching similar results (accuracy=96%, MCC=0.91). When evaluating how many temperature measurement levels are needed for accurate Ω estimates, guidance can be sought from literature on the storage change term, S_c , since both (Ω and S_c) rely on accurate estimation of scalar (temperature for Ω and gas concentration for S_c) profile. ICOS measurement protocols (Montagnani et al., 2018) on S_c measurement configuration suggest that $z_{EC}^{2/3}$ (z_{EC} =EC measurement height) measurement levels are needed for accurate S_c estimation. Our findings here suggest that $z_{EC}^{1/2}$ levels produce already

reasonably accurate results when detecting decoupling with Ω . For instance if $z_{EC} = 20$ m, then four temperature measurement levels would suffice ($20^{1/2} \approx 4$). These measurement levels should be located at heights where the steepest temperature gradients are typically observed (in addition to the EC height), meaning close to the ground and forest canopy top (Peltola et al., 2021a; Schilperoort et al., 2020). However, the optimal measurement configuration is to some degree site-specific (Nicolini et al., 2018) and should be decided on site-by-site basis.

Data availability

Python codes and data needed for reproducing the results shown in this manuscript can be found in Zenodo (<https://doi.org/10.5281/zenodo.14259134>). Additionally, the codes are shared also via Github (https://github.com/OPeltola/EC_Omega_filtering).

References

- Acevedo, O.C., Moraes, O.L.L., Degrazia, G.A., Fitzjarrald, D.R., Manzi, A.O., Campos, J.G., 2009. Is friction velocity the most appropriate scale for correcting nocturnal carbon dioxide fluxes? *Agricul. Forest. Meterol.* 149 (1), 1–10. <http://dx.doi.org/10.1016/j.agrformet.2008.06.014>, URL: <http://www.sciencedirect.com/science/article/pii/S0168192308001962>.
- Alekseychik, P., Mammarella, I., Launiainen, S., Rannik, Ü., Vesala, T., 2013. Evolution of the nocturnal decoupled layer in a pine forest canopy. *Agricul. Forest. Meterol.* 174–175, 15–27. <http://dx.doi.org/10.1016/j.agrformet.2013.01.011>.
- Amiro, B.D., 1990. Drag coefficients and turbulence spectra within three boreal forest canopies. *Bound.-Layer Meteorol.* 52 (3), 227–246. <http://dx.doi.org/10.1007/BF00122088>.
- Arneth, A., Sitch, S., Pongratz, J., Stocker, B.D., Ciais, P., Poulter, B., Bayer, A.D., Bondeau, A., Calle, L., Chini, L.P., Gasser, T., Fader, M., Friedlingstein, P., Kato, E., Li, W., Lindeskog, M., Nabel, J.E.M.S., Pugh, T.A.M., Robertson, E., Viovy, N., Yue, C., Zaehle, S., 2017. Historical carbon dioxide emissions caused by land-use changes are possibly larger than assumed. *Nat. Geosci.* 10 (2), 79–84. <http://dx.doi.org/10.1038/ngeo2882>.
- Arriga, N., Goded, I., Dell'Acqua, A., Matteucci, M., 2020. ETC L2 ARCHIVE, San Rossore 2, 2018-12-31-2020-12-31. URL: https://hdl.handle.net/11676/xsn55wvnOdLD_ta5UE19v42M.

- Aslan, T., Launiainen, S., Kolari, P., Peltola, O., Aalto, J., Bäck, J., Vesala, T., Mammarella, I., 2024. Thinning turned boreal forest to a temporary carbon source - short term effects of partial harvest on carbon dioxide and water vapor fluxes. *Agricult. Forest. Meteorol.* 353, 110061. <http://dx.doi.org/10.1016/j.agrformet.2024.110061>, URL: <https://www.sciencedirect.com/science/article/pii/S016819232400176X>.
- Aubinet, M., 2008. Eddy covariance CO₂ flux measurements in nocturnal conditions: An analysis of the problem. *Ecol. Appl.* 18 (6), 1368–1378. <http://dx.doi.org/10.1890/06-1336.1>, Type: Journal Article.
- Aubinet, M., Berbigier, P., Bernhofer, C.H., Cescatti, A., Feigenwinter, C., Granier, A., Grunwald, T.H., Havrankova, K., Heinesch, B., Longdoz, B., Marcolla, B., Montagnani, L., Sedlak, P., 2005. Comparing CO₂ storage and advection conditions at night at different carboeuroflux sites. *Bound.-Layer Meteorol.* 116 (1), 63–94. <http://dx.doi.org/10.1007/s10546-004-7091-8>, Type: Journal Article.
- Aubinet, M., Feigenwinter, C., Heinesch, B., Bernhofer, C., Canepa, E., Lindroth, A., Montagnani, L., Rebmann, C., Sedlak, P., Van Gorsel, E., 2010. Direct advection measurements do not help to solve the night-time CO₂ closure problem: Evidence from three different forests. *Agricult. Forest. Meteorol.* 150 (5), 655–664. <http://dx.doi.org/10.1016/j.agrformet.2010.01.016>, Type: Journal Article.
- Aubinet, M., Feigenwinter, C., Heinesch, B., Laffineur, Q., Papale, D., Reichstein, M., Rinne, J., Van Gorsel, E., 2012. Nighttime flux correction. In: Aubinet, M., Vesala, T., Papale, D. (Eds.), *Eddy Covariance: A Practical Guide To Measurement and Data Analysis*. Springer Netherlands, Dordrecht, pp. 133–157. http://dx.doi.org/10.1007/978-94-007-2351-1_5, Type: Book Section.
- Aubinet, M., Heinesch, B., Yernaux, M., 2003. Horizontal and vertical CO₂ advection in a sloping forest. *Bound.-Layer Meteorol.* 108 (3), 397–417. <http://dx.doi.org/10.1023/A:1024168428135>.
- Aurela, M., Lohila, A., Tuovinen, J.P., Hatakka, J., Penttilä, T., Laurila, T., 2015. Carbon dioxide and energy flux measurements in four northern-boreal ecosystems at Pallas. *Boreal Environ. Res.* 20, 455–473.
- Baldocchi, D.D., 2020. How eddy covariance flux measurements have contributed to our understanding of global change biology. *Global Change Biol.* 26 (1), 242–260. <http://dx.doi.org/10.1111/gcb.14807>, Publisher: John Wiley & Sons, Ltd.
- Barr, A.G., Richardson, A.D., Hollinger, D.Y., Papale, D., Arain, M.A., Black, T.A., Bohrer, G., Dragoni, D., Fischer, M.L., Gu, L., Law, B.E., Margolis, H.A., McCaughey, J.H., Munger, J.W., Oechel, W., Schaeffer, K., 2013. Use of change-point detection for friction-velocity threshold evaluation in eddy-covariance studies. *Agricult. Forest. Meteorol.* 171–172, 31–45. <http://dx.doi.org/10.1016/j.agrformet.2012.11.023>, URL: <https://www.sciencedirect.com/science/article/pii/S0168192312003607>.
- Belcher, S.E., Finnigan, J.J., Harman, I.N., 2008. Flows through forest canopies in complex terrain. *Ecol. Appl.* 18 (6), 1436–1453. <http://dx.doi.org/10.1890/06-1894.1>, Publisher: John Wiley & Sons, Ltd.
- Belcher, S.E., Jerram, N., Hunt, J.C.R., 2003. Adjustment of a turbulent boundary layer to a canopy of roughness elements. *J. Fluid Mech.* 488, 369–398. <http://dx.doi.org/10.1017/S0022112003005019>, URL: <https://www.cambridge.org/core/article/adjustment-of-a-turbulent-boundary-layer-to-a-canopy-of-roughness-elements/8D5C3E3DFD6A0D3325B3AA824FD59D39>. Edition: 2003/07/02 Publisher: Cambridge University Press.
- Bougeault, P., Lacarrere, P., 1989. Parameterization of orography-induced turbulence in a mesobeta-scale model. *Mon. Weather Rev.* 117 (8), 1872–1890. [http://dx.doi.org/10.1175/1520-0493\(1989\)117<1872:POOITI>2.0.CO;2](http://dx.doi.org/10.1175/1520-0493(1989)117<1872:POOITI>2.0.CO;2), URL: https://journals.ametsoc.org/view/journals/mwre/117/8/1520-0493_117_1872_pooiti_2_0_co_2.xml. Place: Boston MA, USA Publisher: American Meteorological Society.
- Brown, L.A., Meier, C., Morris, H., Pastor-Guzman, J., Bai, G., Lerebours, C., Gobron, N., Lanconelli, C., Clerici, M., Dash, J., 2020. Evaluation of global leaf area index and fraction of absorbed photosynthetically active radiation products over North America using Copernicus ground based observations for validation data. *Remote Sens. Environ.* 247, 111935. <http://dx.doi.org/10.1016/j.rse.2020.111935>, URL: <https://www.sciencedirect.com/science/article/pii/S0034425720303059>.
- Brown, L.A., Morris, H., Leblanc, S., Bai, G., Lanconelli, C., Gobron, N., Meier, C., Dash, J., 2023. HemPy: A Python module for automated estimation of forest biophysical variables and uncertainties from digital hemispherical photographs. *Methods Ecol. Evol.* 14 (9), 2329–2340. <http://dx.doi.org/10.1111/2041-210X.14199>, Publisher: John Wiley & Sons, Ltd.
- Brunet, Y., 2020. Turbulent flow in plant canopies: Historical perspective and overview. *Bound.-Layer Meteorol.* 177 (2), 315–364. <http://dx.doi.org/10.1007/s10546-020-00560-7>.
- Cava, D., Katul, G.G., Sempreviva, A.M., Giostra, U., Scrimieri, A., 2008. On the anomalous behaviour of scalar flux-variance similarity functions within the canopy sub-layer of a dense alpine forest. *Bound.-Layer Meteorol.* 128 (1), 33. <http://dx.doi.org/10.1007/s10546-008-9276-z>.
- Chen, B., Chamecki, M., Katul, G.G., 2019. Effects of topography on in-canopy transport of gases emitted within dense forests. *Q. J. R. Meteorol. Soc.* 145 (722), 2101–2114. <http://dx.doi.org/10.1002/qj.3546>, Publisher: John Wiley & Sons, Ltd.
- Cionco, R.M., 1965. A mathematical model for air flow in a vegetative canopy. *J. Appl. Meteorol. Climatol.* 4 (4), 517–522. [http://dx.doi.org/10.1175/1520-0450\(1965\)004<517:AMMFAC>2.0.CO;2](http://dx.doi.org/10.1175/1520-0450(1965)004<517:AMMFAC>2.0.CO;2), URL: https://journals.ametsoc.org/view/journals/apme/4/4/1520-0450_004_0517_ammfac_2_0_co_2.xml. Place: Boston MA, USA Publisher: American Meteorological Society.
- Cramer, F., Shephard, G.E., Heron, P.J., 2020. The misuse of colour in science communication. *Nature Commun.* 11 (1), 5444. <http://dx.doi.org/10.1038/s41467-020-19160-7>.
- Dufrêne, E., Delpierre, N., Morfin, A., Vincent, G., Bazot, S., Soudani, K., Berveiller, D., 2020. ETC L2 ARCHIVE, Fontainebleau-Barbeau, 2018-12-31–2020-12-31. URL: https://hdl.handle.net/11676/iAES_z8kPfTowb_K9OrD9J-w.
- Dyer, A.J., 1974. A review of flux-profile relationships. *Bound.-Layer Meteorol.* 7 (3), 363–372. <http://dx.doi.org/10.1007/BF00240838>.
- Feigenwinter, C., Bernhofer, C., Eichelmann, U., Heinesch, B., Hertel, M., Janous, D., Kolle, O., Lagergren, F., Lindroth, A., Minerbi, S., Moderow, U., Molder, M., Montagnani, L., Queck, R., Rebmann, C., Vestin, P., Yernaux, M., Zeri, M., Ziegler, W., Aubinet, M., 2008. Comparison of horizontal and vertical advective CO₂ fluxes at three forest sites. *Agricult. Forest. Meteorol.* 148 (1), 12–24. <http://dx.doi.org/10.1016/j.agrformet.2007.08.013>, Type: Journal Article.
- Feigenwinter, C., Bernhofer, C., Vogt, R., 2004. The influence of advection on the short term CO₂-budget in and above a forest canopy. *Bound.-Layer Meteorol.* 113 (2), 201–224. <http://dx.doi.org/10.1023/B:BOUN.0000039372.86053.ff>.
- Feigenwinter, C., Mölder, M., Lindroth, A., Aubinet, M., 2010. Spatiotemporal evolution of CO₂ concentration, temperature, and wind field during stable nights at the Norunda forest site. *Agricult. Forest. Meteorol.* 150 (5), 692–701. <http://dx.doi.org/10.1016/j.agrformet.2009.08.005>, URL: <http://www.sciencedirect.com/science/article/pii/S016819230900197X>.
- Finnigan, J., 2000. Turbulence in plant canopies. *Annu. Rev. Fluid Mech.* 32 (1), 519–571. <http://dx.doi.org/10.1146/annurev.fluid.32.1.519>, Publisher: Annual Reviews.
- Finnigan, J., 2006. The storage term in eddy flux calculations. *Agricult. Forest. Meteorol.* 136 (3–4), 108–113. <http://dx.doi.org/10.1016/j.agrformet.2004.12.010>, Type: Journal Article.
- Finnigan, J.J., Clement, R., Malhi, Y., Leuning, R., Cleugh, H., 2003. A re-evaluation of long-term flux measurement techniques - Part I: Averaging and coordinate rotation. *Bound.-Layer Meteorol.* 107 (1), 1–48. <http://dx.doi.org/10.1023/A:1021554900225>.
- Foken, T., Aubinet, M., Leuning, R., 2012. The Eddy covariance method. In: Aubinet, M., Vesala, T., Papale, D. (Eds.), *Eddy Covariance*. In: Springer Atmospheric Sciences, Springer Netherlands, pp. 1–19. http://dx.doi.org/10.1007/978-94-007-2351-1_1, Section 1 Type: Book Section.
- Franz, D., Acosta, M., Altimir, N., Arriga, N., Arrouays, D., Aubinet, M., Aurela, M., Ayres, E., Lopez-Ballesteros, A., Barbaste, M., Berveiller, D., Biraud, S., Boukir, H., Brown, T., Bruemmer, C., Buchmann, N., Burba, G., Carrara, A., Cescatti, A., Ceschia, E., Clement, R., Cremonese, E., Crill, P., Darenova, E., Dengel, S., D'Odorico, P., Filippa, G., Fleck, S., Fratini, G., Fuss, R., Gielen, B., Gogo, S., Grace, J., Graf, A., Grelle, A., Gross, P., Gruenwald, T., Haapanala, S., Hehn, M., Heinesch, B., Heiskanen, J., Herbst, M., Herschlein, C., Hortnagl, L., Huffkens, K., Ibrom, A., Jolivet, C., Joly, L., Jones, M., Kiese, R., Klemeditsson, L., Kljun, N., Klumpp, K., Kolari, P., Kolle, O., Kowalski, A., Kutsch, W., Laurila, T., de Ligne, A., Linder, S., Lindroth, A., Lohila, A., Longdoz, B., Mammarella, I., Manise, T., Maranon Jimenez, S., Matteucci, G., Mauder, M., Meier, P., Merbold, L., Mereu, S., Metzger, S., Migliavacca, M., Molder, M., Montagnani, L., Moureaux, C., Nelson, D., Nemitz, E., Nicolini, G., Nilsson, M.B., de Beeck, M., Osborne, B., Lofvenius, M.O., Pavelka, M., Peichl, M., Peltola, O., Pihlatie, M., Pitacco, A., Pokorny, R., Pumpanen, J., Ratje, C., Rebmann, C., Roland, M., Sabbatini, S., Saby, N.P.A., Saunders, M., Schmid, H.P., Schrumpf, M., Sedlak, P., Serrano Ortiz, P., Siebke, L., Sigut, L., Silvennoinen, H., Simioni, G., Skiba, U., Sonnentag, O., Soudani, K., Soule, P., Steinbrecher, R., Tallec, T., Thimonier, A., Tuittila, E.S., Tuovinen, J.P., Vestin, P., Vincent, G., Vincke, C., Vitale, D., Waldner, P., Weslien, P., Wingate, L., Wohlfahrt, G., Zahniser, M., Vesala, T., 2018. Towards long-term standardised carbon and greenhouse gas observations for monitoring Europe's terrestrial ecosystems: a review. *Int. Agrophysics* 32 (4), 439+. <http://dx.doi.org/10.1515/intag-2017-0039>, Place: BOGUMILA ZUGA 32A STR., 01-811 WARSAW, POLAND Publisher: DE GRUYTER POLAND SP ZOO Type: Review.
- Freundorfer, A., Rehberg, I., Law, B.E., Thomas, C., 2019. Forest wind regimes and their implications on cross-canopy coupling. *Agricult. Forest. Meteorol.* 279, 107696. <http://dx.doi.org/10.1016/j.agrformet.2019.107696>, URL: <http://www.sciencedirect.com/science/article/pii/S0168192319303120>.
- Galvagno, M., Wohlfahrt, G., Cremonese, E., Filippa, G., Migliavacca, M., Mora di Cellia, U., van Gorsel, E., 2017. Contribution of advection to nighttime ecosystem respiration at a mountain grassland in complex terrain. *Agricult. Forest. Meteorol.* 237–238, 270–281. <http://dx.doi.org/10.1016/j.agrformet.2017.02.018>, URL: <https://www.sciencedirect.com/science/article/pii/S0168192317300515>.
- Gharun, M., Baur, T., Etzold, S., Eugster, W., Gessler, A., Hug, C., Häni, M., Hörtnagl, L., Kumar, S., Liechti, K., Marty, M., Meier, P., Schmitt Oehler, M., Stutz, T., Sutter, F., Thimonier Rickenmann, A., Waldner, P., Zimmermann, S., Zweifel, R., 2020. ETC L2 ARCHIVE, Davos, 2018-12-31–2020-12-31. URL: <https://hdl.handle.net/11676/9PY7uZwJdXy9WWpWgp45lk5>.
- Ghisalberti, M., 2009. Obstructed shear flows: similarities across systems and scales. *J. Fluid Mech.* 641, 51–61. <http://dx.doi.org/10.1017/S0022112009992175>, URL: <https://www.cambridge.org/core/article/obstructed-shear-flows-similarities-across-systems-and-scales/57CB658F47B27DB2A24B03236B3AD25B>. Edition: 2009/12/10 Publisher: Cambridge University Press.

- Gielen, B., Acosta, M., Altimir, N., Buchmann, N., Cescatti, A., Ceschia, E., Fleck, S., Hörtnagl, L., Klumpp, K., Kolari, P., Lohila, A., Loustau, D., Marañon-Jimenez, S., Manise, T., Matteucci, G., Merbold, L., Metzger, C., Moureaux, C., Montagnani, L., Nilsson, M.B., Osborne, B., Papale, D., Pavelka, M., Saunders, M., Simioni, G., Soudani, K., Sonnentag, O., Tallec, T., Tuittila, E.S., Peichl, M., Pokorny, R., Vincke, C., Wohlfahrt, G., 2018. Ancillary vegetation measurements at ICOS ecosystem stations. *Int. Agrophys.* 32 (4), 645–664. <http://dx.doi.org/10.1515/intag-2017-0048>.
- van Gorsel, E., Delpierre, N., Leuning, R., Black, A., Munger, J.W., Wofsy, S., Aubinet, M., Feigenwinter, C., Beringer, J., Bonal, D., Chen, B., Chen, J., Clement, R., Davis, K.J., Desai, A.R., Dragoni, D., Etzold, S., Grünwald, T., Gu, L., Heinesch, B., Hutyra, L.R., Jans, W.W.P., Kutsch, W., Law, B.E., Leclerc, M.Y., Mammarella, I., Montagnani, L., Noormets, A., Rebmann, C., Wharton, S., 2009. Estimating nocturnal ecosystem respiration from the vertical turbulent flux and change in storage of CO₂. *Agricul. Forest. Meteorol.* 149 (11), 1919–1930. <http://dx.doi.org/10.1016/j.agrformet.2009.06.020>, URL: <https://www.sciencedirect.com/science/article/pii/S0168192309001634>.
- van Gorsel, E., Harman, I.N., Finnigan, J.J., Leuning, R., 2011. Decoupling of air flow above and in plant canopies and gravity waves affect micrometeorological estimates of net scalar exchange. *Agricul. Forest. Meteorol.* 151 (7), 927–933. <http://dx.doi.org/10.1016/j.agrformet.2011.02.012>, URL: <http://www.sciencedirect.com/science/article/pii/S0168192311000785>.
- Goulden, M.L., Munger, J.W., Fan, S.M., Daube, B.C., Wofsy, S.C., 1996. Measurements of carbon sequestration by long-term eddy covariance: Methods and a critical evaluation of accuracy. *Global Change Biol.* 2 (3), 169–182. <http://dx.doi.org/10.1111/j.1365-2486.1996.tb00070.x>, Type: Journal Article.
- Gu, L., Falge, E.M., Boden, T., Baldocchi, D.D., Black, T.A., Saleska, S.R., Suni, T., Verma, S.B., Vesala, T., Wofsy, S.C., Xu, L., 2005. Objective threshold determination for nighttime eddy flux filtering. *Agricul. Forest. Meteorol.* 128 (3), 179–197. <http://dx.doi.org/10.1016/j.agrformet.2004.11.006>, URL: <http://www.sciencedirect.com/science/article/pii/S0168192304003053>.
- Harman, I.N., Finnigan, J.J., 2007. A simple unified theory for flow in the canopy and roughness sublayer. *Bound.-Layer Meteorol.* 123 (2), 339–363. <http://dx.doi.org/10.1007/s10546-006-9145-6>.
- Harman, I.N., Finnigan, J.J., 2008. Scalar concentration profiles in the canopy and roughness sublayer. *Bound.-Layer Meteorol.* 129 (3), 323–351. <http://dx.doi.org/10.1007/s10546-008-9328-4>.
- Heiskanen, J., Brümmer, C., Buchmann, N., Calfapietra, C., Chen, H., Gielen, B., Gkrizalis, T., Hammer, S., Hartman, S., Herbst, M., Janssens, I.A., Jordan, A., Juurula, E., Karstens, U., Kasurinen, V., Kruyt, B., Lankreijer, H., Levin, I., Linderson, M.L., Loustau, D., Merbold, L., Myhre, C.L., Papale, D., Pavelka, M., Pilegaard, K., Ramonet, M., Rebmann, C., Rinne, J., Rivier, L., Saltikoff, E., Sanders, R., Steinbacher, M., Steinhoff, T., Watson, A., Vermeulen, A.T., Vesala, T., Vítková, G., Kutsch, W., 2022. The integrated carbon observation system in Europe. *Bull. Am. Meteorol. Soc.* 103 (3), E855–E872. <http://dx.doi.org/10.1175/BAMS-D-19-0364.1>, URL: <https://journals.ametsoc.org/view/journals/bams/103/3/BAMS-D-19-0364.1.xml>. Place: Boston MA, USA Publisher: American Meteorological Society.
- Heliaas, M., Biermann, T., Holst, J., Holst, T., Linderson, M.L., Mölder, M., Rinne, J., 2020. ETC L2 ARCHIVE, Hylitemossa, 2017-12-31–2020-12-31. URL: <https://hdl.handle.net/11676/w4Usod0iDifPg-IHhvPYBggv>.
- Huntingzinger, D.N., Michalak, A.M., Schwalm, C., Ciais, P., King, A.W., Fang, Y., Schaefer, K., Wei, Y., Cook, R.B., Fisher, J.B., Hayes, D., Huang, M., Ito, A., Jain, A.K., Lei, H., Lu, C., Maignan, F., Mao, J., Parazoo, N., Peng, S., Poultre, B., Ricciuto, D., Shi, X., Tian, H., Wang, W., Zeng, N., Zhao, F., 2017. Uncertainty in the response of terrestrial carbon sink to environmental drivers undermines carbon-climate feedback predictions. *Sci. Rep.* 7 (1), 4765. <http://dx.doi.org/10.1038/s41598-017-03818-2>.
- Inoue, E., 1963. On the turbulent structure of airflow within crop canopies. *J. Meteorol. Soc. Japan. Ser. II* 41 (6), 317–326. http://dx.doi.org/10.2151/jmsj1923.41_6_317.
- Jammet, M., Dengel, S., Kettner, E., Parmentier, F.J.W., Wik, M., Crill, P., Friberg, T., 2017. Year-round CH₄ and CO₂ flux dynamics in two contrasting freshwater ecosystems of the subarctic. *Biogeosciences* 14 (22), 5189–5216. <http://dx.doi.org/10.5194/bg-14-5189-2017>, URL: <https://www.biogeosciences.net/14/5189/2017/>. Publisher: Copernicus Publications.
- Jocher, G., Fischer, M., Šigut, L., Pavelka, M., Sedláček, P., Katul, G., 2020. Assessing decoupling of above and below canopy air masses at a Norway spruce stand in complex terrain. *Agricul. Forest. Meteorol.* 294, 108149. <http://dx.doi.org/10.1016/j.agrformet.2020.108149>, URL: <http://www.sciencedirect.com/science/article/pii/S0168192320302513>.
- Jocher, G., Ottosson Löfvenius, M., De Simon, G., Hörlund, T., Linder, S., Lundmark, T., Marshall, J., Nilsson, M.B., Näsholm, T., Tarvainen, L., Öquist, M., Peichl, M., 2017. Apparent winter CO₂ uptake by a boreal forest due to decoupling. *Agricul. Forest. Meteorol.* 232, 23–34. <http://dx.doi.org/10.1016/j.agrformet.2016.08.002>, Publisher: Elsevier.
- Kaimal, J.C., Finnigan, J.J., 1994. Atmospheric boundary layer flows : their structure and measurement. Oxford University Press, New York, URL: <http://helka.linneanet.fi/cgi-bin/Pwebrecogn.cgi?BBID=636956>. Type: Book.
- Kanani-Sühring, F., Raasch, S., 2015. Spatial variability of scalar concentrations and fluxes downstream of a clearing-to-forest transition: A large-eddy simulation study. *Bound.-Layer Meteorol.* 155 (1), 1–27. <http://dx.doi.org/10.1007/s10546-014-9986-3>.
- Kanani-Sühring, F., Raasch, S., 2017. Enhanced scalar concentrations and fluxes in the lee of forest patches: A large-eddy simulation study. *Bound.-Layer Meteorol.* 164 (1), 1–17. <http://dx.doi.org/10.1007/s10546-017-0239-0>.
- Katul, G.G., Finnigan, J.J., Poggi, D., Leuning, R., Belcher, S.E., 2006. The influence of hilly terrain on canopy-atmosphere carbon dioxide exchange. *Bound.-Layer Meteorol.* 118 (1), 189–216. <http://dx.doi.org/10.1007/s10546-005-6436-2>, Type: Journal Article.
- Knohl, A., Tiedemann, F., Markwitz, C., Siebicke, L., 2021. ETC L2 ARCHIVE, Hainich, 2018-12-31–2020-12-31. URL: https://hdl.handle.net/11676/WiCY4SuszNzoell_SJugCrXDM.
- Kunadi, A.S., Silberstein, R.P., Thompson, S.E., 2024. Variation in zero plane displacement and roughness length for momentum revisited. *Bound.-Layer Meteorol.* 190 (8), 36. <http://dx.doi.org/10.1007/s10546-024-00876-8>.
- Kutsch, W.L., Kolle, O., Rebmann, C., Knohl, A., Ziegler, W., Schulze, E.-D., 2008. Advection and resulting CO₂ exchange uncertainty in a tall forest in central Germany. *Ecol. Appl.* 18 (6), 1391–1405. <http://dx.doi.org/10.1890/06-1301.1>, Publisher: John Wiley & Sons, Ltd.
- Lac, C., Chaboureau, J.P., Masson, V., Pinty, J.P., Tulet, P., Escobar, J., Leriche, M., Barthe, C., Aouizerats, B., Augros, C., Aumond, P., Auguste, F., Bechtold, P., Berthet, S., Bielli, S., Bosseur, F., Caumont, O., Cohard, J.M., Colin, J., Couvreux, F., Cuxart, J., Delautier, G., Dauhut, T., Ducrocq, V., Filippi, J.B., Gazen, D., Geoffroy, O., Gheusi, F., Honnert, R., Lafore, J.P., Lebeaupin Brossier, C., Libois, Q., Lunet, T., Mari, C., Maric, T., Mascart, P., Mogé, M., Molinié, G., Nuissier, O., Pantillon, F., Peyrillé, P., Pergaud, J., Perraud, E., Pineazze, J., Redelsperger, J.L., Ricard, D., Richard, E., Riette, S., Rodier, Q., Schoetter, R., Seyfried, L., Stein, J., Suhre, K., Taufour, M., Thouron, O., Turner, S., Verrelle, A., Vié, B., Visentin, F., Vionnet, V., Wautelet, P., 2018. Overview of the Meso-NH model version 5.4 and its applications. *Geosci. Model Dev.* 11 (5), 1929–1969. <http://dx.doi.org/10.5194/gmd-11-1929-2018>, URL: <https://gmd.copernicus.org/articles/11/1929/2018/gmd-11-1929-2018.pdf>. Publisher: Copernicus Publications.
- Leuning, R., Zegelin, S.J., Jones, K., Keith, H., Hughes, D., 2008. Measurement of horizontal and vertical advection of CO₂ within a forest canopy. *Agricul. Forest. Meteorol.* 148 (11), 1777–1797. <http://dx.doi.org/10.1016/j.agrformet.2008.06.006>, URL: <https://www.sciencedirect.com/science/article/pii/S016819230800186X>.
- Li, D., Salesky, S.T., Banerjee, T., 2016. Connections between the Ozmidov scale and mean velocity profile in stably stratified atmospheric surface layers. *J. Fluid Mech.* 797, R3. <http://dx.doi.org/10.1017/jfm.2016.311>, URL: <https://www.cambridge.org/core/article/connections-between-the-ozmidov-scale-and-mean-velocity-profile-in-stably-stratified-atmospheric-surface-layers/8FC6918C8A541A494D29B70D839145F>. Edition: 2016/05/24 Publisher: Cambridge University Press.
- Lohila, A., Aurela, M., Tuovinen, J.P., Laurila, T., 2004. Annual CO₂ exchange of a peat field growing spring barley or perennial forage grass. *J. Geophys. Res.: Atmos.* 109 (D18), <http://dx.doi.org/10.1029/2004JD004715>, Publisher: John Wiley & Sons, Ltd.
- Loustau, D., Aluome, C., Chipeaux, C., Denou, J.L., Kruszewski, A., Lafont, S., 2020. ETC L2 ARCHIVE, Bilos, 2018-12-31–2020-12-31. URL: <https://hdl.handle.net/11676/J9dwIEpZs3JB1vsW13VbRyHe>.
- Ma, Y., Liu, H., Liu, Z., Yi, C., Lamb, B., 2020. Influence of forest-edge flows on scalar transport with different vertical distributions of foliage and scalar sources. *Bound.-Layer Meteorol.* 174 (1), 99–117. <http://dx.doi.org/10.1007/s10546-019-00475-y>.
- Mahrt, L., 1979. Penetrative convection at the top of a growing boundary layer. *Q. J. R. Meteorol. Soc.* 105 (444), 469–485. <http://dx.doi.org/10.1002/qj.49710544411>, Publisher: John Wiley & Sons, Ltd.
- Mahrt, L., Richardson, S., Seaman, N., Stauffer, D., 2012. Turbulence in the nocturnal boundary layer with light and variable winds. *Q. J. R. Meteorol. Soc.* 138 (667), 1430–1439. <http://dx.doi.org/10.1002/qj.1884>, Type: Journal Article.
- Mahrt, L., Sun, J., Blumen, W., Delany, T., Oncley, S., 1998. Nocturnal boundary-layer regimes. *Bound.-Layer Meteorol.* 88 (2), 255–278, Type: Journal Article.
- Mammarella, I., Back, J., Kolari, P., Laakso, H., Levula, J., Matilainen, T., Pihlatie, M., Pumpanen, J., Taipale, R., Vesala, T., 2021. ETC L2 ARCHIVE, Hyttiala, 2017-12-31–2020-12-31. URL: https://hdl.handle.net/11676/Nn_zvmRQW4i7iq3U8D3jNCRO.
- Mammarella, I., Kolari, P., Rinne, J., Keronen, P., Pumpanen, J., Vesala, T., 2007. Determining the contribution of vertical advection to the net ecosystem exchange at Hyttiälä forest, Finland. *Tellus B* 59 (5), 900–909. <http://dx.doi.org/10.1111/j.1600-0889.2007.00306.x>, Publisher: Taylor & Francis.
- Marcolla, B., Cescatti, A., Montagnani, L., Manca, G., Kerschbaumer, G., Minerbi, S., 2005. Importance of advection in the atmospheric CO₂ exchanges of an alpine forest. *Agricul. Forest. Meteorol.* 130 (3–4), 193–206. <http://dx.doi.org/10.1016/j.agrformet.2005.03.006>, Type: Journal Article.
- Maroneze, R., Acevedo, O.C., Costa, F.D., Puhalles, F.S., Anabor, V., Lemes, D.N., Mortarini, L., 2020. How is the two-regime stable boundary layer reproduced by the different turbulence parametrizations in the weather research and forecasting model? *Bound.-Layer Meteorol.* <http://dx.doi.org/10.1007/s10546-020-00581-2>.

- Metzger, S., Ayres, E., Durden, D., Florian, C., Lee, R., Lunch, C., Luo, H., Pingintha-Durden, N., Roberti, J.A., SanClements, M., Sturtevant, C., Xu, K., Zulueta, R.C., 2019. From NEON field sites to data portal: A community resource for surface-atmosphere research comes online. *Bull. Am. Meteorol. Soc.* 100 (11), 2305–2325. <http://dx.doi.org/10.1175/BAMS-D-17-0307.1>, URL: <https://journals.ametsoc.org/view/journals/bams/100/11/bams-d-17-0307.1.xml>. Place: Boston MA, USA Publisher: American Meteorological Society.
- Metzger, S., Durden, D., Sturtevant, C., Luo, H., Pingintha-Durden, N., Sachs, T., Serafimovich, A., Hartmann, J., Li, J., Xu, K., Desai, A.R., 2017. eddy4R 0.2.0: a DevOps model for community-extensible processing and analysis of eddy-covariance data based on R, Git, Docker, and HDF5. *Geosci. Model Dev.* 10 (9), 3189–3206. <http://dx.doi.org/10.5194/gmd-10-3189-2017>, URL: <https://gmd.copernicus.org/articles/10/3189/2017/https://gmd.copernicus.org/articles/10/3189/2017/gmd-10-3189-2017.pdf>. Publisher: Copernicus Publications.
- Mölder, M., Lehner, I., Bäth, A., Holst, J., Linderson, M.L., 2020. ETC L2 ARCHIVE, Norunda, 2017-12-31–2020-12-31. URL: <https://hdl.handle.net/11676/BtuSQuDRWOCeHouJDbViHUpo>.
- Monin, A., Obukhov, A., 1954. Basic laws of turbulent mixing in the atmosphere near the ground. *Trudy Geofiz Inst AN SSSR* 24, 163–187.
- Montagnani, L., Grünwald, T., Kowalski, A., Mammarella, I., Merbold, L., Metzger, S., Sedláć, P., Siebicke, L., 2018. Estimating the storage term in eddy covariance measurements: the ICOS methodology. *Int. Agrophys.* 32 (4), 551–567. <http://dx.doi.org/10.1515/intag-2017-0037>.
- Moum, J.N., 1996. Energy-containing scales of turbulence in the ocean thermocline. *J. Geophys. Res.: Oceans* 101 (C6), 14095–14109. <http://dx.doi.org/10.1029/96JC00507>, Publisher: John Wiley & Sons, Ltd.
- National Ecological Observatory Network (NEON), 2022. Digital hemispheric photos of plot vegetation (DP1.10017.001). <http://dx.doi.org/10.48443/X12V-N568>, URL: <https://data.neonscience.org/data-products/DP1.10017.001/RELEASE-2022>.
- National Ecological Observatory Network (NEON), 2023. Bundled data products - eddy covariance (DP4.00200.001). <http://dx.doi.org/10.48443/2MS3-A333>, URL: <https://data.neonscience.org/data-products/DP4.00200.001/RELEASE-2023>.
- Neff, H., Ghisalberti, M., White, B., Murphy, E., 2007. Retention time and dispersion associated with submerged aquatic canopies. *Water Resour. Res.* 43 (4), <http://dx.doi.org/10.1029/2006WR005362>, Publisher: John Wiley & Sons, Ltd.
- Nicolini, G., Aubinet, M., Feigenwinter, C., Heinesch, B., Lindroth, A., Mamadou, O., Moderow, U., Mölder, M., Montagnani, L., Rebmann, C., Papale, D., 2018. Impact of CO₂ storage flux sampling uncertainty on net ecosystem exchange measured by eddy covariance. *Agricul. Forest. Meteorol.* 248, 228–239. <http://dx.doi.org/10.1016/j.agrformet.2017.09.025>, URL: <https://www.sciencedirect.com/science/article/pii/S0168192317303209>.
- Nilsson, M., Peichl, M., Marklund, P., De Simon, G., Smith, P., Löfvenius, P., Dignam, R., Holst, J., Mölder, M., Andersson, T., Linderson, M.L., Lindgren, K., 2020. ETC L2 ARCHIVE, Degerö, 2018-12-31–2020-12-31. URL: <https://hdl.handle.net/11676/Pyl6-HjdM0-zHaPhTYYHOBYz>.
- Papale, D., Reichstein, M., Aubinet, M., Canfora, E., Bernhofer, C., Kutsch, W., Longdoz, B., Rambal, S., Valentini, R., Vesala, T., Yakir, D., 2006. Towards a standardized processing of Net Ecosystem Exchange measured with eddy covariance technique: algorithms and uncertainty estimation. *Biogeosciences* 3 (4), 571–583. <http://dx.doi.org/10.5194/bg-3-571-2006>, URL: <https://bg.copernicus.org/articles/3/571/2006/bg-3-571-2006.pdf>. Publisher: Copernicus Publications.
- Pastorello, G., Trotta, C., Canfora, E., Chu, H., Christianson, D., Cheah, Y.W., Poindexter, C., Chen, J., Elbashandy, A., Humphrey, M., Isaac, P., Polidori, D., Reichstein, M., Ribeca, A., van Ingen, C., Vuichard, N., Zhang, L., Amiro, B., Ammann, C., Arain, M.A., Ardö, J., Arkebauer, T., Arndt, S.K., Arriga, N., Aubinet, M., Aurela, M., Baldocchi, D., Barr, A., Beamesderfer, E., Marchesini, L.B., Bergeron, O., Beringer, J., Bernhofer, C., Berveiller, D., Billesbach, D., Black, T.A., Blanken, P.D., Bohrer, G., Boike, J., Bolstad, P.V., Bonal, D., Bonnefond, J.-M., Bowling, D.R., Bracho, R., Brodeur, J., Brümmer, C., Buchmann, N., Burban, B., Burns, S.P., Buissey, P., Cale, P., Cavagna, M., Cellier, P., Chen, S., Chini, I., Christensen, T.R., Cleverly, J., Collalti, A., Consalvo, C., Cook, B.D., Cook, D., Coursolle, C., Cremonese, E., Curtiss, P.S., D'Andrea, E., da Rocha, H., Dai, X., Davis, K.J., Cinti, B.D., de Grandcourt, A., Ligne, A.D., de Oliveira, R.C., Delpierre, N., Desai, A.R., Di Bella, C.M., di Tommasi, P., Dolman, H., Domingo, F., Dong, G., Dore, S., Duce, P., Dufrêne, E., Dunn, A., Dušek, J., Eamus, D., Eichelmann, U., ElKhidir, H.A.M., Eugster, W., Ewenz, C.M., Ewers, B., Famulari, D., Fares, S., Feigenwinter, I., Feitz, A., Fensholt, R., Filippa, G., Fischer, M., Frank, J., Galvagno, M., Gharun, M., Gianelle, D., Gielen, B., Gioli, B., Gitelson, A., Goded, I., Goedcke, M., Goldstein, A.H., Gough, C.M., Goulden, M.L., Graf, A., Griebel, A., Gruening, C., Grünwald, T., Hammerle, A., Han, S., Han, X., Hansen, B.U., Hanson, C., Hatakka, J., He, Y., Hehn, M., Heinesch, B., Hinko-Najera, N., Hörtnagl, L., Hutley, L., Ibrom, A., Ikawa, H., Jackowicz-Korczynski, M., Janouš, D., Jans, W., Jassal, R., Jiang, S., Kato, T., Khomik, M., Klatt, J., Knohl, A., Knox, S., Kobayashi, H., Koerber, G., Kolle, O., Kosugi, Y., Kotani, A., Kowalski, A., Kruijt, B., Kurbatova, J., Kutsch, W.L., Kwon, H., Launiainen, S., Laurila, T., Law, B., Leuning, R., Li, Y., Liddell, M., Limousin, J.M., Lion, M., Liska, A.J., Lohila, A., López-Ballesteros, A., López-Blanco, E., Loubet, B., Loutsau, D., Lucas-Moffat, A., Lüters, J., Ma, S., Macfarlane, C., Magliulo, V., Maier, R., Mammarella, I., Manca, G., Marcolla, B., Margolis, H.A., Marras, S., Massman, W., Mastepanov, M., Matamala, R., Matthes, J.H., Mazzenga, F., McCaughey, H., McHugh, I., McMillan, A.M.S., Merbold, L., Meyer, W., Meyers, T., Miller, S.D., Minerbi, S., Moderow, U., Monson, R.K., Montagnani, L., Moore, C.E., Moors, E., Moreaux, V., Moureaux, C., Munger, J.W., Nakai, T., Neirynck, J., Nesic, Z., Nicolini, G., Noormets, A., Northwood, M., Noysetto, M., Nouvellon, Y., Novick, K., Oechel, W., Olesen, J.R.E., Ourcival, J.M., Papuga, S.A., Parmentier, F.J., Paul-Limoges, E., Pavelka, M., Peichl, M., Pendall, E., Phillips, R.P., Pilegaard, K., Pirk, N., Posse, G., Powell, T., Prasse, H., Prober, S.M., Rambal, S., Rannik, Ü., Raz-Yaseef, N., Rebmann, C., Reed, D., de Dios, V.R., Restrepo-Coupe, N., Reverter, B.R., Roland, M., Sabbatini, S., Sachs, T., Saleska, S.R., Sánchez-Cañete, E.P., Sanchez-Mejia, Z.M., Schmid, H.P., Schmidt, M., Schneider, K., Schrader, F., Schroder, I., Scott, R.L., Sedláć, P., Serrano-Ortíz, P., Shao, C., Shi, P., Shironya, I., Siebicke, L., Sigut, L., Silberstein, R., Sirca, C., Spano, D., Steinbrecher, R., Stevens, R.M., Sturtevant, C., Suyker, A., Tagesson, T., Takanashi, S., Tang, Y., Tapper, N., Thom, J., Tomassucci, M., Tuovinen, J.-P., Urbanski, S., Valentini, R., van der Molen, M., van Gorsel, E., van Huissteden, K., Varlagin, A., Verfaillie, J., Vesala, T., Vincke, C., Vitale, D., Vygodskaya, N., Walker, J.P., Walter-Shea, E., Wang, H., Weber, R., Westermann, S., Wille, C., Wofsy, S., Wohlfahrt, G., Wolf, S., Woodgate, W., Li, Y., Zampedri, R., Zhang, J., Zhou, G., Zona, D., Agarwal, D., Biraud, S., Torn, M., Papale, D., 2020. The FLUXNET2015 dataset and the ONEflux processing pipeline for eddy covariance data. *Sci. Data* 7 (1), 225. <http://dx.doi.org/10.1038/s41597-020-0534-3>.
- Peichl, M., Nilsson, M., Smith, P., Marklund, P., De Simon, G., Löfvenius, P., Dignam, R., Holst, J., Mölder, M., Andersson, T., Linderson, M.L., Ottosson-Löfvenius, M., Tülp, H., Öquist, M., 2020. ETC L2 ARCHIVE, Svarterget, 2018-12-31–2020-12-31. URL: <https://hdl.handle.net/11676/QfqUnGlc6UY4Fb8bCdQbjMB>.
- Peltola, O., Aurela, M., Launiainen, S., Katul, G., 2022. Probing eddy size and its effective mixing length in stably stratified roughness sublayer flows. *Q. J. R. Meteorol. Soc.* 148 (749), <http://dx.doi.org/10.1002/qj.4386>, Publisher: John Wiley & Sons, Ltd.
- Peltola, O., Lapo, K., Martinkuuppi, I., O'Connor, E., Thomas, C.K., Vesala, T., 2021a. Suitability of fibre-optic distributed temperature sensing for revealing mixing processes and higher-order moments at the forest-air interface. *Atmos. Meas. Tech.* 14 (3), 2409–2427. <http://dx.doi.org/10.5194/amt-14-2409-2021>, URL: <https://amt.copernicus.org/articles/14/2409/2021/amt-14-2409-2021.pdf>. Publisher: Copernicus Publications.
- Peltola, O., Lapo, K., Thomas, C.K., 2021b. A physics-based universal indicator for vertical decoupling and mixing across canopies architectures and dynamic stabilities. *Geophys. Res. Lett.* 48 (5), <http://dx.doi.org/10.1029/2020GL091615>, e2020GL091615. Publisher: Wiley Online Library.
- Platter, A., Scholz, K., Hammerle, A., Rotach, M.W., Wohlfahrt, G., 2024. Agreement of multiple night- and daytime filtering approaches of eddy covariance-derived net ecosystem CO₂ exchange over a mountain forest. *Agricul. Forest. Meteorol.* 356, 110173. <http://dx.doi.org/10.1016/j.agrformet.2024.110173>, URL: <https://www.sciencedirect.com/science/article/pii/S0168192324002867>.
- Poggi, D., Katul, G.G., 2007. Turbulent flows on forested hilly terrain: the recirculation region. *Q. J. R. Meteorol. Soc.* 133 (625), 1027–1039. <http://dx.doi.org/10.1002/qj.73>, Publisher: John Wiley & Sons, Ltd.
- Poggi, D., Porporato, A., Ridolfi, L., Albertson, J.D., Katul, G.G., 2004. The effect of vegetation density on canopy sub-layer turbulence. *Bound.-Layer Meteorol.* 111 (3), 565–587. <http://dx.doi.org/10.1023/B:BOUN.0000016576.05621.73>.
- Rannik, Ü., Vesala, T., Peltola, O., Novick, K.A., Aurela, M., Järvi, L., Montagnani, L., Mölder, M., Peichl, M., Pilegaard, K., Mammarella, I., 2020. Impact of coordinate rotation on eddy covariance fluxes at complex sites. *Agricul. Forest. Meteorol.* 287, 107940. <http://dx.doi.org/10.1016/j.agrformet.2020.107940>, URL: <https://www.sciencedirect.com/science/article/pii/S0168192320300423>.
- Rebmann, C., Dienstbach, L., Schmidt, P., Garcia Quiros, I., Gimper, S., 2020. ETC L2 ARCHIVE, Hohes Holz, 2018-12-31–2020-12-31. URL: https://hdl.handle.net/11676/hWDTopTdjCZlmQu3t_QmOBJ.
- Reichstein, M., Falge, E., Baldocchi, D., Papale, D., Aubinet, M., Berbigier, P., Bernhofer, C., Buchmann, N., Gilmanov, T., Granier, A., Grünwald, T., Havránková, K., Ilvesniemi, H., Janous, D., Knöhl, A., Laurila, T., Lohila, A., Loustau, D., Matteucci, G., Meyers, T., Miglietta, F., Ourcival, J.-M., Pumpanen, J., Rambal, S., Rotenberg, E., Sanz, M., Tenhunen, J., Seufert, G., Vaccari, F., Vesala, T., Yakir, D., Valentini, R., 2005. On the separation of net ecosystem exchange into assimilation and ecosystem respiration: review and improved algorithm. *Global Change Biol.* 11 (9), 1424–1439. <http://dx.doi.org/10.1111/j.1365-2486.2005.001002.x>, Publisher: Wiley/Blackwell (10.1111).
- Ross, A.N., 2011. Scalar transport over forested hills. *Bound.-Layer Meteorol.* 141 (2), 179–199. <http://dx.doi.org/10.1007/s10546-011-9628-y>.
- Ross, A.N., Harman, I.N., 2015. The impact of source distribution on scalar transport over forested hills. *Bound.-Layer Meteorol.* 156 (2), 211–230. <http://dx.doi.org/10.1007/s10546-015-0029-5>.
- Sabbatini, S., Mammarella, I., Arriga, N., Fratini, G., Graf, A., Hörrnagl, L., Ibrom, A., Longdoz, B., Mauder, M., Merbold, L., Metzger, S., Montagnani, L., Pitacco, A., Rebmann, C., Sedláć, P., Sigut, L., Vitale, D., Papale, D., 2018. Eddy covariance raw data processing for CO₂ and energy fluxes calculation at ICOS ecosystem stations. *Int. Agrophys.* 32, 495–515. <http://dx.doi.org/10.1515/intag-2017-0043>.

- Schilperoort, B., Coenders-Gerrits, M., Jiménez Rodríguez, C., van der Tol, C., van de Wiel, B., Savenije, H., 2020. Decoupling of a Douglas fir canopy: a look into the subcanopy with continuous vertical temperature profiles. *Biogeosciences* 17 (24), 6423–6439. <http://dx.doi.org/10.5194/bg-17-6423-2020>, Publisher: Copernicus Publications.
- Siebcke, L., Hunner, M., Foken, T., 2012. Aspects of CO₂ advection measurements. *Theor. Appl. Climatol.* 109 (1), 109–131. <http://dx.doi.org/10.1007/s00704-011-0552-3>.
- Sorbian, Z., 2006. Local structure of turbulence in stably stratified boundary layers. *J. Atmos. Sci.* 63 (5), 1526–1537. <http://dx.doi.org/10.1175/JAS3704.1>.
- Staebler, R.M., Fitzjarrald, D.R., 2004. Observing subcanopy CO₂ advection. *Agricul. Forest. Meterol.* 122 (3–4), 139–156. <http://dx.doi.org/10.1016/j.agrformet.2003.09.011>, Type: Journal Article.
- Stiegler, C., June, T., Markwitz, C., Camarretta, N., Ali, A.A., Knohl, A., 2023. Wind regimes above and below a dense oil palm canopy: Detection of decoupling and its implications on CO₂ flux estimates. *Agricul. Forest. Meterol.* 341, 109668. <http://dx.doi.org/10.1016/j.agrformet.2023.109668>, URL: <https://www.sciencedirect.com/science/article/pii/S0168192323003581>.
- Tallec, T., Ceschia, E., Granouillac, F., Claverie, N., Zawilski, B., Brut, A., Lemaire, B., Gibrin, H., 2021. ETC L2 ARCHIVE, Aurade, 2018-12-31–2020-12-31. URL: https://hdl.handle.net/11676/BiCe9kHD_o-jBOQ1lpAGwK6o.
- Thomas, C.K., 2011. Variability of sub-canopy flow, temperature, and horizontal advection in moderately complex terrain. *Bound.-Layer Meteorol.* 139 (1), 61–81. <http://dx.doi.org/10.1007/s10546-010-9578-9>.
- Thomas, C.K., Martin, J.G., Law, B.E., Davis, K., 2013. Toward biologically meaningful net carbon exchange estimates for tall, dense canopies: Multi-level eddy covariance observations and canopy coupling regimes in a mature Douglas-fir forest in Oregon. *Agricul. Forest Meterol.* 173, 14–27. <http://dx.doi.org/10.1016/j.agrformet.2013.01.001>, Publisher: Elsevier.
- Thum, T., Aalto, T., Laurila, T., Aurela, M., Kolari, P., Hari, P., 2007. Parametrization of two photosynthesis models at the canopy scale in a northern boreal Scots pine forest. *Tellus B* 59 (5), 874–890. <http://dx.doi.org/10.1111/j.1600-0889.2007.00305.x>, Publisher: John Wiley & Sons, Ltd.
- Van Gorsel, E., Leuning, R., Cleugh, H., Keith, H., Suni, T., 2007. Nocturnal carbon efflux: reconciliation of eddy covariance and chamber measurements using an alternative to the u*-threshold filtering technique. *Tellus B* 59 (3), 397–403. <http://dx.doi.org/10.1111/j.1600-0889.2007.00252.x>, Publisher: John Wiley & Sons, Ltd.
- Vickers, D., Irvine, J., Martin, J.G., Law, B.E., 2012. Nocturnal subcanopy flow regimes and missing carbon dioxide. *Agricul. Forest. Meterol.* 152, 101–108. <http://dx.doi.org/10.1016/j.agrformet.2011.09.004>, URL: <http://www.sciencedirect.com/science/article/pii/S0168192311002802>.
- Wutzler, T., Lucas-Moffat, A., Migliavacca, M., Knauer, J., Sickel, K., Šigut, L., Menzer, O., Reichstein, M., 2018. Basic and extensible post-processing of eddy covariance flux data with REddyProc. *Biogeosciences* 15 (16), 5015–5030. <http://dx.doi.org/10.5194/bg-15-5015-2018>, Publisher: Copernicus GmbH.
- Xu, K., Pinginha-Durden, N., Luo, H., Durden, D., Sturtevant, C., Desai, A.R., Florian, C., Metzger, S., 2019. The eddy-covariance storage term in air: Consistent community resources improve flux measurement reliability. *Agricul. Forest. Meterol.* 279, 107734. <http://dx.doi.org/10.1016/j.agrformet.2019.107734>, URL: <https://www.sciencedirect.com/science/article/pii/S0168192319303508>.
- Yi, C., 2008. Momentum transfer within canopies. *J. Appl. Meteorol. Climatol.* 47 (1), 262–275. <http://dx.doi.org/10.1175/2007JAMC1667.1>.